

Chapter 4 – Reactor Description ATOMIC ALCHEMY INC.

Non-Proprietary

Document Number	Revision	Approved By	Template
AAI-PSAR-04 (NP)	0		TEM-003 Rev 2 (05/14/2025)



TABLE OF CONTENTS

Te	erms .			4-4
	Abbr	eviatio	ns and Acronyms	4-4
4	Re	actor [Description	4-5
	4.0	Intro	duction	4-5
	4.1	Sumr	mary Description	4-5
	4.2	Reac	tor Core	4-8
	4.2	2.1	Reactor Fuel	4-8
	4.2	2.2	Control Rods	4-11
	4.2	2.3	Neutron Moderator and Reflector	4-19
		4.2.3.1	Primary Coolant	4-19
		4.2.3.2	DANK Tank	4-20
		4.2.3.3	Beryllium Neutron Reflector	4-21
	4.2	2.4	Neutron Startup Source	4-22
	4.2	2.5	Core Support Structure	4-22
	4.3	Reac	tor Pool	4-25
	4.4	Biolo	gical Shielding	4-26
	4.5	Nucle	ear Design	4-30
	4.5	5.1	Normal Operating Conditions	4-30
		4.5.1.1	Core Components	4-30
		4.5.1.2	Core Configurations	4-31
	4.5	5.2	Reactor Core Physics Parameters	4-33
		4.5.2.1	Neutron Lifetime and Delayed Neutron Fraction	4-33
		4.5.2.2	Reactivity Coefficients	4-35
		4.5.2.3	Power Distribution	4-38
	4.5	5.3	Operating Limits	4-42
		4.5.3.1	Reactivity Limits	4-42
		4.5.3.2	Limiting Core Configuration	4-43
	4.6	Theri	mal-Hydraulic Design	4-43
	4.6	5.1	Design Criteria	4-43
		4.6.1.1	Nominal Core Configuration	4-44
		4.6.1.2	Limiting Core Configuration	4-44



AAI-PSAR-04 (NP) Rev 0 Page 4-2

4.6.1.3 Fuel Characteristics	4-45
4.6.2 Methodology	4-46
4.6.2.1 Models	4-46
4.6.2.2 Uncertainty	4-50
4.6.3 Steady-State Analysis	4-51
4.6.3.1 Forced Convection Mode	4-51
4.6.3.2 Natural Convection Mode	4-52
4.6.3.3 Transients and Power Pulses	4-55
4.7 References	
LIST OF FIGURES	
Figure 4-1: Isometric rendering of the VIPR	4-6
Figure 4-2: Isometric rendering of the VIPR without the DANK tank	4-6
Figure 4-3: Side view drawing of the VIPR fuel assembly (dimensions in in	nches)4-9
Figure 4-4: Top-down isometric rendering of a VIPR fuel assembly	4-10
Figure 4-5: Side view drawing of the VIPR fuel pin (dimensions in inches)	4-10
Figure 4-6: Top-down isometric rendering of the VIPR core	4-12
Figure 4-7: Side-view of the VIPR control rod assembly (dimensions in in	•
Figure 4-8: Side-view of a VIPR control rod (dimensions in inches)	
Figure 4-9: Top-down view of the VIPR control rod assembly (dimension	
Figure 4-10: Integral worth of an individual control rod assembly	
Figure 4-11: Integral worth of all control rod assemblies	
Figure 4-12: Integral worth of all rod assemblies minus the most reactive	•
Figure 4-13: Integral worth of the regulating rod assembly	
Figure 4-14: Isometric rendering of the core support structure	
Figure 4-15: Stress model of the core support structure	
Figure 4-16: Displacement model of the core support structure	
Figure 4-17: Transfer canal-side isometric view of the biological baryte s	_
Figure 4-18: Auxiliary pit-side isometric view of the biological baryte ship	
Figure 4-19: XZ and YZ cross sections of the VIPR pool and shielding	
Figure 4-20: Fuel cycle excess reactivity in limiting and steady state conf Figure 4-21: Reactivity change as a function of average fuel temperature	_
Figure 4-21: Reactivity change as a function of average rule temperature	
Figure 4-23: Reactivity change as a function of primary coolant temperary Figure 4-23: Reactivity change as a function of primary coolant void fraction.	
Figure 4-24: Qualitative depiction of the VIPR pin-wise power distribution	
Figure 4-25: Axial power distribution in the hot pin and bulk fuel	
Figure 4-26: Nodal diagram of the RELAP5 model for the VIPR core and F	
Figure 4-27: RELAP5 nodal diagram of the VIPR core and pool	
Figure 4-28: RELAP5 detailed model of the VIPR core	
Figure 4-29: Temperature profile of a planned shutdown with forced flow	



AAI-PSAR-04 (NP) Rev 0 Page 4-3

Figure 4-30. Temperature profile transition between forced flow and natural convection 4-54
Figure 4-31: Temperature profile of a loss of power event with natural circulation
LIST OF TABLES
Table 4-1: Summary table of important reactor parameters
Table 4-2: Total integral worths of the control rod assemblies in various configurations 4-15
Table 4-3: Operational reactivity requirements
Table 4-4: Total dose rates around the reactor pool
Table 4-5: Core configuration reactivity characteristics
Table 4-6: Delayed neutron fractions (β) and decay constants (λ) for the limiting configuration 4-33
Table 4-7: Delayed neutron fractions (β) and decay constants (λ) for the steady state configuration 4-34
Table 4-8: Total, prompt, and delayed neutron lifetimes for the limiting cycle4-34
Table 4-9: Total, prompt, and delayed neutron lifetimes for the steady state cycle4-34
Table 4-10: Temperature-dependent reactivity coefficients at the beginning of the limiting cycle 4-37
Table 4-11: Parameters used in the iterative calculation of the reactor's power, temperature, and
density distributions4-39
Table 4-12: Nominal interdependent variables for designed steady state operation 4-44
Table 4-13: Reactor core parameters4-44
Table 4-14: Wall convection heat transfer mode numbers, reproduced from the RELAP5 manual 4-50
Table 4-15: Thermal-hydraulic characteristics of the VIPR core and hot pin
LIST OF FOLIATIONS
LIST OF EQUATIONS
Equation 4-1: Axial coolant temperatures as a function of fuel pin linear heat generation rate 4-38
Equation 4-2: Axial fuel temperatures as a function of fuel pin linear heat generation rate 4-38
Equation 4-3: UO ₂ thermal conductivity fit
Equation 4-4: Light water density fit4-39
Equation 4-5: Pretransition oxidation layer thickness correlation
Equation 4-6: Post-transition oxidation layer thickness correlation



AAI-PSAR-04 (NP) Rev 0 Page 4-4

TERMS

ABBREVIATIONS AND ACRONYMS

Common acronyms, abbreviations, and units of measurements may not be included here as it is assumed the reader is familiar with their meaning.

AAI Atomic Alchemy Inc.

AgInCd silver indium cadmium alloy

CHF critical heat flux

CRDM control rod drive mechanism

DANK deuterium-augmented nuclear kinetics

DNBR departure from nucleate boiling ratio

EPRI Electric Power Research Institute

Gd₂O₃ gadolinium(III) oxide

LEU low-enriched uranium

NIST National Institute of Standards and Technology

PCM percent mille, a unit of reactivity

PCS primary coolant system

PWR pressurized water reactor

SAR Safety Analysis Report

Sm-149 Samarium-149

SCS secondary coolant system

TR topical report

UO₂ uranium dioxide

VIPR Versatile Isotope Production Reactor

Xe-135 Xenon-135



AAI-PSAR-04 (NP) Rev 0 Page 4-5

4 REACTOR DESCRIPTION

4.0 INTRODUCTION

This chapter of the Safety Analysis Report (SAR) describes the principal features, operating characteristics, and parameters of the Atomic Alchemy Inc. (AAI) Versatile Isotope Production Reactor (VIPR). The analyses in this chapter support the conclusion that the VIPR is conservatively designed for safe operation and shutdown under all credible operating conditions.

This chapter, along with the information presented in Chapters 11 and 13, demonstrates that normal operation or the consequences of any other credible condition will not cause unacceptable risk to the health and safety of the public.

Justification for technical specifications for the Systems, Structures, and Components in this chapter are provided in Chapter 14 and will be discussed in the FSAR.

4.1 SUMMARY DESCRIPTION

The VIPR is a 15 MWth reactor designed by AAI to produce radioisotopes for medical, industrial, space, defense, and research applications. The fuel for the VIPR is low-enriched uranium (LEU), enriched up to []PROP,ECI U-235 by weight, in the form of uranium dioxide (UO₂) pins contained in fuel assemblies that are installed on a grid plate. A tank of heavy water surrounds the reactor core radially to provide neutron moderation and reflection; a block of beryllium metal is installed in the center of the core to provide additional moderation and reflection. The heavy water tank is called the deuterium-augmented nuclear kinetics (DANK) tank. A rendering of the VIPR with the inlet piping and DANK tank is shown in **Figure 4-1**. **Figure 4-2** shows the VIPR without the DANK tank allowing the plenum beneath the core to be seen.



AAI-PSAR-04 (NP) Rev 0 Page 4-6

[]PROP,ECI

Figure 4-1: Isometric rendering of the VIPR

[]PROP,ECI

Figure 4-2: Isometric rendering of the VIPR without the DANK tank

Light water serves as both coolant and a neutron moderator and removes heat from the system through forced upwards convection directed through the grid plate. The low thermal power of the VIPR allows for the reactor to be contained in an open pool which facilitates access to the core during its operation. Light water-filled tubes in the heavy water reflector and channels in the center beryllium



AAI-PSAR-04 (NP) Rev 0 Page 4-7

reflector allow for the insertion of irradiation targets to utilize the peak thermal neutron flux and are accessible via automatic or manual manipulation from above the open pool. Neutron leakage at the core periphery is utilized to produce select isotopes or for other auxiliary services, including silicon transmutation doping. Important parameters are summarized in **Table** 4-1.

Table 4-1: Summary table of important reactor parameters

Parameter	Value
Thermal Power Level	15 MWth
Fuel Type	LEU
Fuel enrichment	[]PROP,ECI
Reactor type	Pool
Cooling Type	Upward forced flow
Coolant	Light water
Moderator	Light water
Reflector	Beryllium/Heavy water
Power type	Steady

Reactor power and long-term reactivity changes are actively managed by the variable positioning of neutron-absorbing control rod and regulating rod assemblies within several of the fuel assemblies. The control and regulating rods, as well as the instrumentation necessary for the operation of the reactor, are suspended from a bridge above the surface of the reactor pool and are monitored and controlled by a remote operator.

Short-term changes in reactor power are managed by a number of well-characterized physical effects, particularly thermal reactivity feedback effects in the fuel and the moderator, which make the VIPR inherently safe. The predominant fuel temperature feedback effect is a consequence of the use of LEU fuel, which has a strong Doppler broadening effect in the resonance absorption peaks of U-238 as a response to power changes. Additionally, the large heat capacity of the ceramic UO_2 fuel permits large releases of energy under transient conditions without compromising the integrity of the fuel or cladding. Finally, changes in reactor power cause temperature and density changes in the moderator which result in a negative reactivity feedback. The fuel assemblies used in the VIPR are [

The most significant reactor transient, apart from startup and shutdown, occurs with the deliberate insertion or removal of high-reactivity irradiation targets while the system is operational. These target movements are planned and executed to ensure that no reactivity limits are exceeded, and that the operating reactor is maintained in a safe state.

Heat produced in the core is removed by the forced circulation of pool water upwards through the core to the pool. The primary coolant is cooled by a secondary coolant in a heat exchanger before



AAI-PSAR-04 (NP) Rev 0 Page 4-8

passing through the reactor core. A portion of the returning primary water is continuously filtered and demineralized before being returned. The low power of the reactor and the forced upward flow during operation allow for the VIPR to be cooled by natural convection when shutdown without a flow reversal. As the VIPR core is contained in an open pool and cooled by upward flow, a nitrogen-16 (N-16) suppression system is required to mitigate the release of the short-lived gaseous radionuclide from the coolant. The biological shield serves to physically support and contain the light water pool and shield facility workers from radiation in proximity to the VIPR. Penetrations in the biological shield are made for the primary coolant inlet and outlet.

The AAI facility is designed to accommodate the installation of four VIPR units, each of which are connected to a common water canal that provides access for the movement of irradiated targets to the centralized processing module.

4.2 REACTOR CORE

4.2.1 Reactor Fuel

The following objectives reflect the design bases of the VIPR fuel:

- 1. Maintaining fuel integrity under all conditions up to those assumed in the accident analyses presented in Chapter 13. Loss of fuel integrity is defined as the escape of any fission products from the cladding.
- 2. Damage to the reactor fuel is never so severe as to prevent the insertion of control rods when required.
- 3. Coolability of the fuel must be maintained under all conditions.

The VIPR core contains []PROP,ECI identical fuel assemblies, eac	h a shorter variant of the []PROP,ECI
designed by []PROP,ECI. The VIPR fuel assemblies are	similar to those used in [
] ^{PROP} in most param	eters except the height of the active	fuel region and the number ar	nd location
of the fuel pin spacer grid	ds. Departures from the standard []PROP design or VIPR impleme	entation-
specific features include:			

Active fuel and fuel assembly length
 The height of the active fuel region of the VIPR core is [] PROP,ECI. The total length of each assembly including the hardware at the ends of the fuel pins and the assembly end structures is [] PROP,ECI. The transverse dimensions of the fuel assembly and its envelope remain unchanged.

Fuel enrichment
 All fuel pellets in the VIPR core are uniformly enriched to []PROP,ECI U-235.

• Burnable poison concentration and location

Among the fuel pins, $[\]^{PROP,ECI}$ in each fuel assembly contain fuel pellets uniformly doped to $[\]^{PROP,ECI}$ gadolinium(III) oxide (Gd_2O_3) burnable poison to provide passive long-term reactivity control. The Gd_2O_3 containing fuel pins are regularly located throughout the fuel assembly, as shown in **Figure 4-4**.



AAI-PSAR-04 (NP) Rev 0 Page 4-9

• Guide tube utilization

[]PROP,ECI fuel assemblies contain either control or regulating rod assemblies; in those fuel assemblies that do not contain control elements the guide tubes are left empty.

Spacer grid frequency and type

A side view drawing showing top and bottom nozzle assemblies, fuel pin spacer grids, and the orientation of the fuel pins is shown in **Figure 4-3**. A top-down rending of a VIPR fuel assembly containing fuel pins (yellow), fuel pins with burnable poisons (orange), inserted control rods (green), and an empty central guide tube is shown in **Figure 4-4**.

[]PROP,ECI

Figure 4-3: Side view drawing of the VIPR fuel assembly (dimensions in inches)



AAI-PSAR-04 (NP) Rev 0 Page 4-10

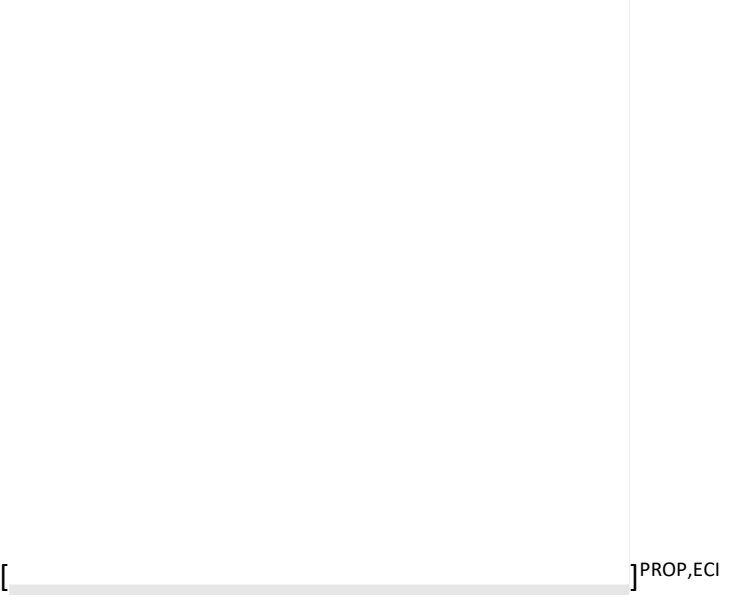


Figure 4-4: Top-down isometric rendering of a VIPR fuel assembly

All fuel pellets in the VIPR core are uniformly enriched to [] PROP,ECI U-235. The active fuel length of each fuel pin is [] PROP,ECI with a total fuel pin length of [] PROP,ECI. A side view drawing of a VIPR fuel pin showing the upper plenum and spring, the fuel stack, and the cladding and end caps is shown in **Figure 4-5**.

[PROP,ECI

Figure 4-5: Side view drawing of the VIPR fuel pin (dimensions in inches)

The use of the ceramic UO₂ with a low enrichment of U-235 results in several layers of defense in depth and passive feedback effects inherent in the fuel, including:

- Strong Doppler feedback effect
 - The low enrichment of U-235 corresponds to a relatively high concentration of U-238, the capture of neutrons in which does not significantly contribute to the fission chain reaction. An increase in the temperature of the fuel, resulting from an increase in fission power or a decrease in cooling capability, causes a widening of the resonance peaks in the U-238 neutron absorption cross section and increases the likelihood of neutrons being absorbed in the fuel without causing fissions. This reduces the rate of fission reactions and decreases the reactor power should the fuel temperature unintentionally increase.
- High specific heat capacity



AAI-PSAR-04 (NP) Rev 0

Page 4-11

The high specific heat capacity of UO_2 requires the deposition of greater quantities of energy to cause temperature increases comparable to those experienced by other fuel materials, increasing the resilience of the fuel to power excursions.

High melting temperature

Ceramic UO₂ has a higher melting temperature than other fuel materials, permitting operation and ensuring reliability under a greater range of conditions.

Appro	val of [
_	- ,	. Nuclear Regulatory Commission (NRO PROP,ECT fuel. Specific references to the G-1537 include:	, ·
•	[dimensions, materials, a guide and instrument tu]PROP,ECI gives descriptions of the [and fabrication methods of the fuel assibes, and nozzles.	- 3,
•	- · · · · · · · · · · · · · · · · · · ·] ^{PROP,ECI} provides analyses and results and loading limits; strain fatigue; fretti assembly bow and growth; fuel rod int	ng wear; oxidation, hydriding,
•] PROP,ECI provides analyses and results	relating to fuel rod failure
	including hydriding, clad	lding collapse, and overheating of fuel	pellets.
•] PROP,ECI provides analyses and results	relating to fuel coolability due to
	structural deformation.		
•	[testing programs. [components of the [] ^{PROP,ECI} outlines the fuel assembly me] ^{PROP,ECI} gives opera] ^{PROP,ECI} fuel assembly, including the f	iting experience for specific

4.2.2 Control Rods

bottom nozzles, and guide tubes.

The following objectives reflect the design basis of the control rod assemblies:

- 1. Assurance of the insertion of the control rods into the VIPR core under all conditions up to and including those assumed in the accident analyses presented in Chapter 13.
- 2. Sufficient integral worth of the control rods to shut down the VIPR under all conditions, in compliance with the "one stuck rod" criterion.

The VIPR utilizes control and regulating rod assemblies for the control of reactor power and the compensation of reactivity changes in the core over time. Large changes in reactor power, such as reactor startup and shutdown, and compensation for long-term reactivity changes resulting from fuel burnup and the buildup of fission product poisons are achieved by the movement of the control rod assemblies. The regulating rod assembly provides fine control of the reactor power and compensates



AAI-PSAR-04 (NP) Rev 0 Page 4-12

for short-term reactivity changes, including the movements of irradiation targets into and out of the VIPR core.

Control rod assemblies are installed in each of the [] PROP,ECI fuel assemblies directly adjacent to the central neutron reflector; the regulating rod assembly is installed in one of the remaining corner fuel assemblies. A rendering of how these are located in the cord is shown in **Figure 4-6** along with the core adjacent irradiation facilities.

[PROP,ECI

Figure 4-6: Top-down isometric rendering of the VIPR core

The control rod assemblies utilized in the VIPR core are shortened variants of the [] PROP,ECI. The control rod assemblies are similar to those used in commercial PWRs in most parameters except the height of the silver-indium-cadmium alloy (AgInCdg) neutron absorber region, the design of the plenum spring, and the departure from the use of ion-nitrided cladding.

A side-view drawing of the VIPR implementation of the [] PROP,ECI showing the control rods, spider assembly, and couplings is shown in **Figure 4-7**. A side-view drawing of a VIPR control rod



AAI-PSAR-04 (NP) Rev 0 Page 4-13

showing the upper AgInCd absorber, lower annular AgInCd absorber, plenum, and cladding is shown in **Figure 4-8**. A top-down view drawing of the VIPR implementation of the [] PROP,ECI showing the coupling, spider assembly, and relative positions of the individual control rods is shown in **Figure 4-9**.

Fabrication methods and specifications with tolerances will be provided in the FSAR. Analyses and historical data relating to change in reactivity worth due to burnup, assessments of radiation damage, heating effects, and chemical compatibility with coolant and other core components will also be provided in the FSAR.

[PROP,ECI

Figure 4-7: Side-view of the VIPR control rod assembly (dimensions in inches)

[]PROP,ECI

Figure 4-8: Side-view of a VIPR control rod (dimensions in inches)



AAI-PSAR-04 (NP) Rev 0 Page 4-14

]PROP,ECI

Figure 4-9: Top-down view of the VIPR control rod assembly (dimensions in inches)

Each control rod assembly, consisting of the individual control rods connected to a common spider assembly, is connected to a control rod drive mechanism (CRDM) installed on the bridge spanning the reactor pool. Each CRDM provides vertical movement of its assembly through an electric motor, gear reduction system, and screw drive. The control rod assembly is electromagnetically connected to its CRDM, ensuring that in the event that power is lost or the CRDM fails to actuate the control rods fail safe into the VIPR core.

The total integral worth of the average control rod assembly is 1,824 percent mille (pcm) (2.57 \$); systems around the VIPR core which influence the system neutronics, such as the regulating rod assembly or strongly neutron-absorbing or neutron-producing irradiation targets, produce small variations in the integral and differential worths of each control rod assembly.

The radial symmetry of the control rod assemblies around the VIPR preserves the radial uniformity of the neutron flux in the core. Together, the control rod assemblies have an integral worth of 12,853 pcm (17.92 \$). The arrangement of the control rods around the central neutron reflector effectively



AAI-PSAR-04 (NP) Rev 0 Page 4-15

isolates the reflector from the remainder of the core and partitions the fuel assemblies into subcritical regions, contributing to the significant total worth of the control rods assemblies.

The maximum speed at which the control rods can be withdrawn is 0.17 cm/s, corresponding to a maximum reactivity insertion rate of 69 pcm/s (0.10 \$/s) should all control rod assemblies be simultaneously withdrawn through the region of highest neutron flux. As the neutron absorbing control rods are actuated axially through the approximately cosine-shaped neutron flux distribution in the core, the integral worth of the control rods takes a corresponding sinusoid-shaped curve. The maximum rate of reactivity insertion and removal occurs around the position of the fuel centerline. The average rate of reactivity insertion across the height of the core is 39 pcm/s (0.06 \$/s) for the simultaneous removal of all control rod assemblies at the maximum rate. However, outside of scram insertion of the control rod assemblies, movement of only a single control rod assembly at a given time is permitted.

While the VIPR can be controlled through movement of the control rods alone, the relatively large worth of the ganged clusters makes fine control impractical. An assembly of regulating rods, which are identical to the control rods apart from utilizing 304L stainless steel as the neutron-absorbing material, is located in a single corner fuel assembly. The substitution of the neutron absorber results in a greatly decreased differential rod worth and allows for finer control of the reactivity of the system, as movement of the regulating rod assembly has a much smaller effect than that produced by a comparable movement of a control rod assembly. The regulating rod does not have scram capability and is not credited in any analyses of reactor shutdown or in the calculation of the allowable excess reactivity. The regulating rod mechanism differs from the control rod mechanism in that there is no electromagnet assembly. Instead, it is fixed to its lead screw, therefore, the regulating rod does not drop into the core on receipt of a scram signal.

The control rod assemblies provide sufficient negative reactivity to meet the shutdown margin and maintain the reactor in a shutdown state from the condition with the greatest excess reactivity. Should the highest worth control rod assembly fail to insert into the reactor, the remaining control rods are capable of promptly shutting down the reactor in all conditions; however, the subsequent addition of reactivity from the cooling of the reactor and decay of short-lived neutron poisons may result in a restart of the reactor to a low steady-state power from a limited number of initial reactor conditions. To ensure that the VIPR can be shut down to meet the shutdown margin from any operating condition should the highest worth control rod assembly fail to insert into the core, additional redundancy is provided by the capability to drain heavy water from the adjacent reflector, discussed in Section 4.2.3.2. **Table** 4-2 details the total integral worths of the control rod assemblies in various configurations.

Table 4-2: Total integral worths of the control rod assemblies in various configurations

Configuration	Value	Unit
All Control Rod Assemblies	12,853	pcm
All Control Rod Assemblies, Without Most Reactive	7,022	pcm
All Control Rod Assemblies, Reflector Drained	20,049	pcm



Configuration	Value	Unit
All Control Rod Assemblies, Without Most Reactive, Reflector Drained	12,108	pcm

Plots of the integral worths of an individual control rod assembly, total control rod assemblies, and all but the most reactive control rod assembly as a function of their height above the bottom of the core are shown in **Figure 4-10**, **Figure 4-11**, and **Figure 4-12**, respectively. The integral worth of the regulating rod assembly as a function of its height above the bottom of the core is shown in **Figure 4-13**.

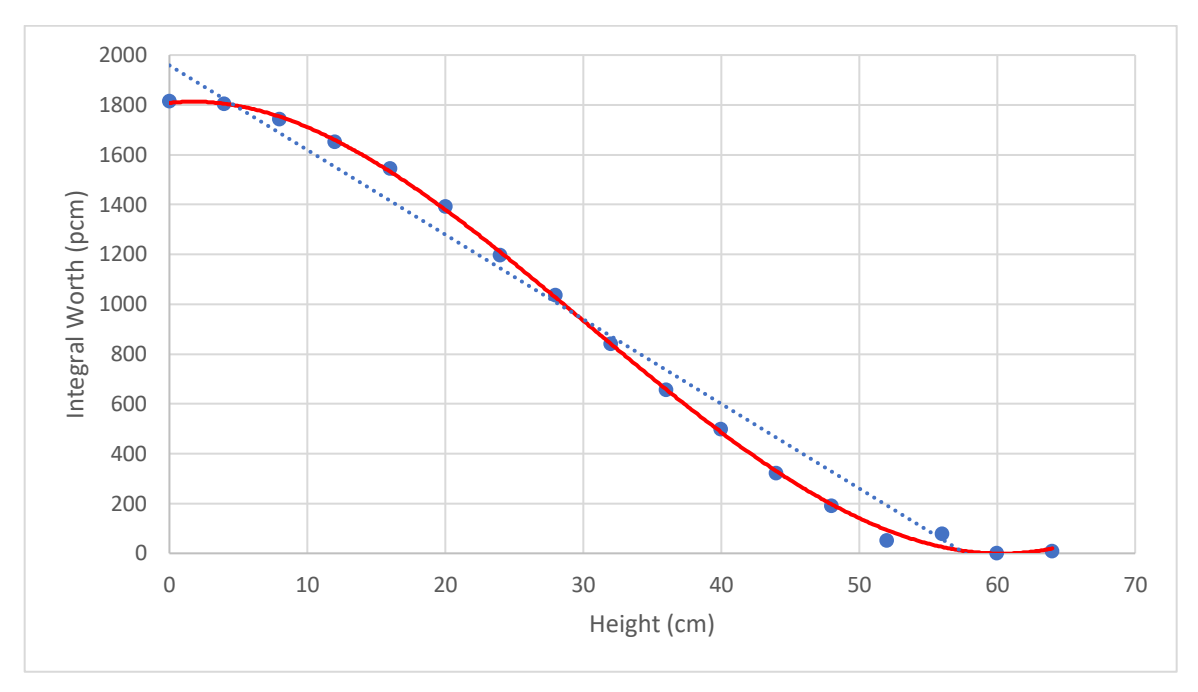
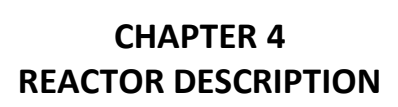


Figure 4-10: Integral worth of an individual control rod assembly





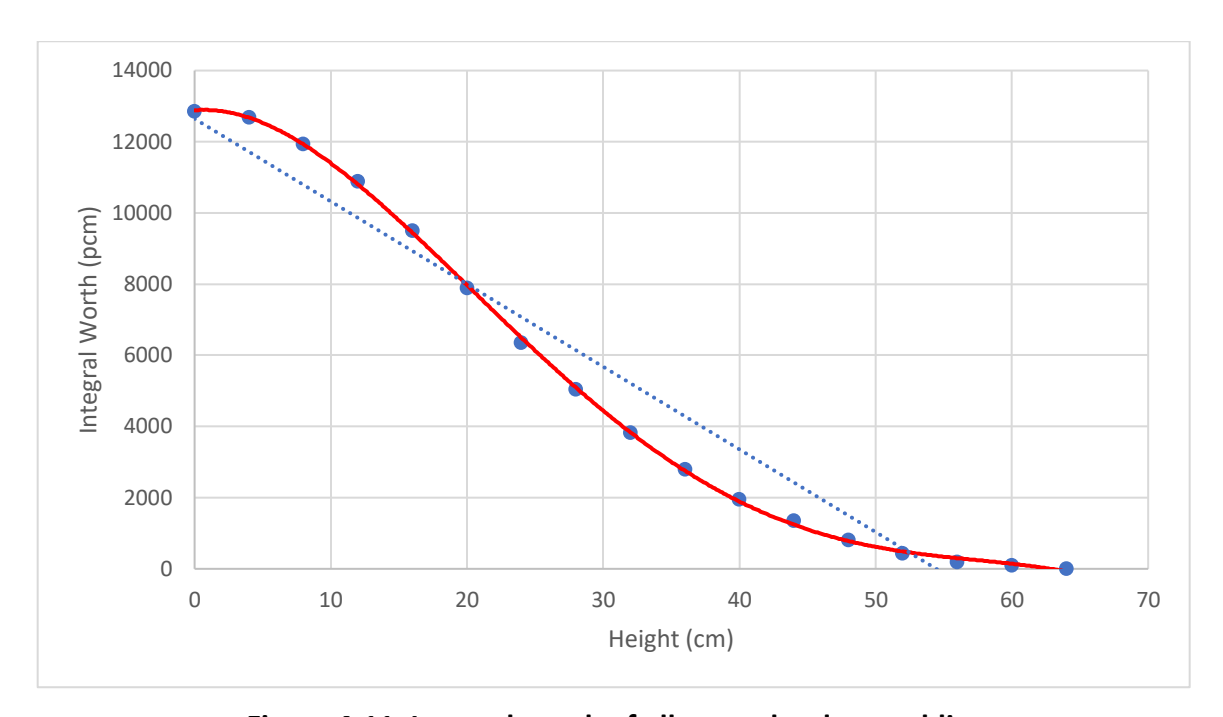


Figure 4-11: Integral worth of all control rod assemblies

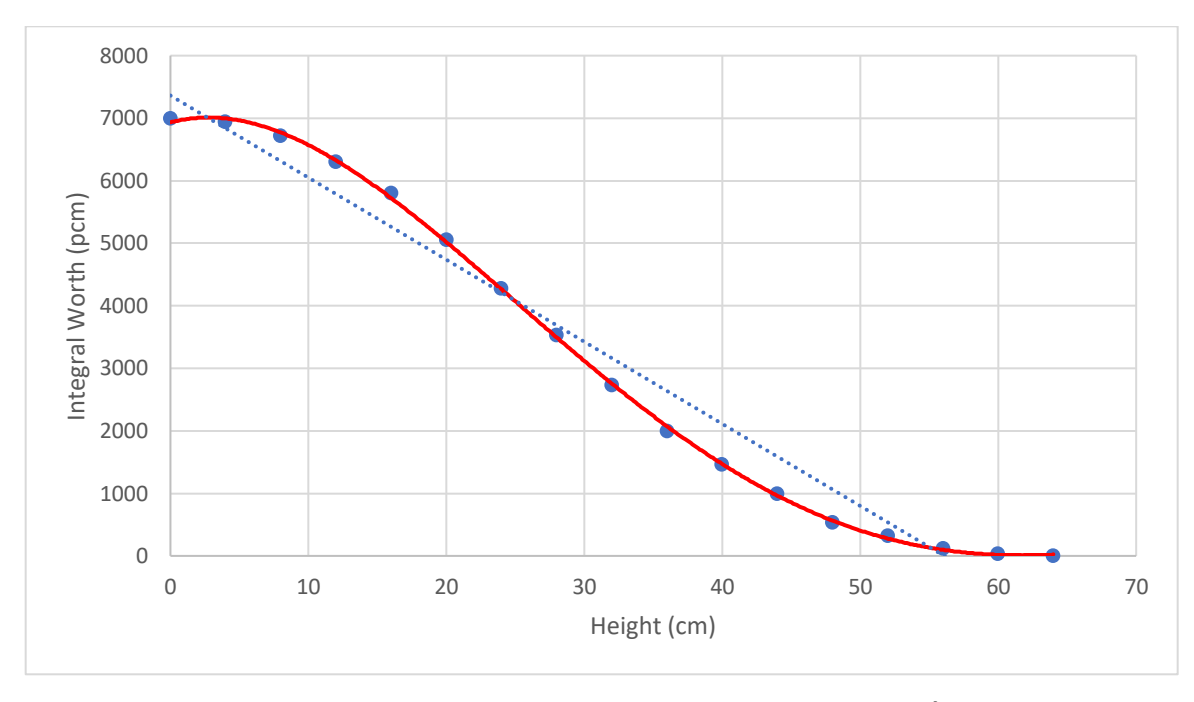


Figure 4-12: Integral worth of all rod assemblies minus the most reactive (one stuck rod criterion)

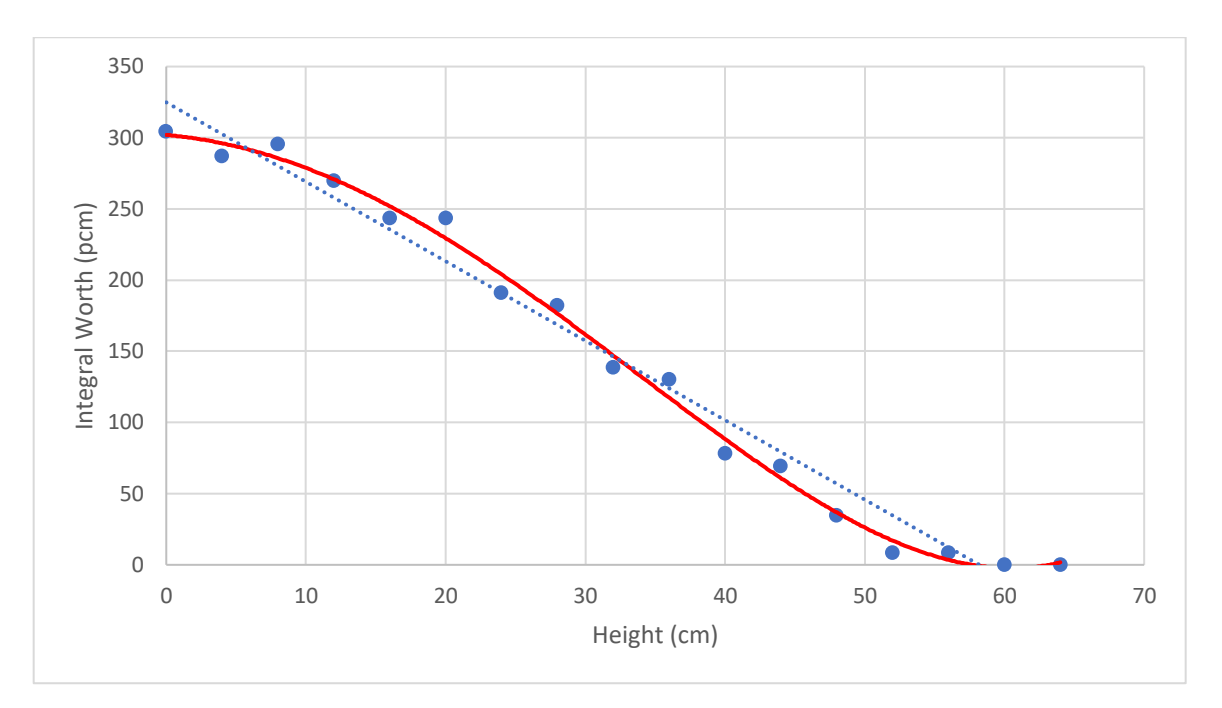


Figure 4-13: Integral worth of the regulating rod assembly

The control rods assemblies are designed to, under the conditions of a reactor scram, fall into the reactor under the force of gravity. This mode of operation includes the case of a loss of power to or mechanical failure of the CRDM. All analyses involving control rod drop kinetics assume the control rod assemblies fall under gravitational acceleration and with a conservative scram delay of 1.0 second.

The determination of a limit on the allowable excess reactivity that may be inserted into the core is essential to ensuring that the reactor can be shut down at any time. The shutdown margin for the reactor in any configuration must be at least 400 pcm (0.56 \$) with the highest worth control rod group completely withdrawn from the core. The calculation of the allowable excess reactivity uses the total worth determined in the "one stuck rod" criterion, rather than simply subtracting the worth of a single control rod group from the total control rod worth. Neither the negative reactivity resulting from the production of xenon and samarium fission product poisons nor the power defect of the reactor are included in the calculations, although calculated values are given in **Table** 4-3, as the control rod worths are evaluated for the most limiting configuration of a fresh core at startup and cannot be credited towards the shutdown of the reactor. These assumptions ensure that the minimum shutdown margin can be met under all postulated conditions.

Table 4-3: Operational reactivity requirements

Parameters	Value	Unit
All Control Rod Assemblies, without most reactive, DANK Tank drained	12,108	pcm
Xenon, Samarium	3,082	pcm
Power Defect	1,174	pcm



AAI-PSAR-04 (NP) Rev 0 Page 4-19

The limit on excess reactivity is obtained by subtracting the requisite shutdown margin from the worth of all the control rod assemblies except the most reactive and a drained DANK tank:

$$12,108 - 400 = 11,708 \text{ pcm}$$

To minimize reliance on heavy water drainage from the DANK tank for reactivity control, the excess reactivity is generally limited to the difference between the total reactivity worth of all control rod assemblies (without the most reactive control rod assembly) with a full DANK tank, and the required shutdown margin:

$$7,022 - 400 = 6,622 \text{ pcm}$$

SCRAM logic, inhibits, interlocks, and initiation systems are described in Chapter 7. The control rods are passive, fail-safe actuators that insert by gravity upon de-energization of their electromagnets when a SCRAM signal is generated by the Reactor Protection System. The credited safety-related function is provided by the Reactor Protection System and the rods insert independently of manufacturing variability or control circuitry. The control rods themselves are classified as non-safety-related.

4.2.3 Neutron Moderator and Reflector

The following objectives reflect the design bases of the neutron moderator and reflector:

- 1. Thermalization of neutrons for increased utilization without over-moderating the system (i.e. leading to positive reactivity feedback coefficients) under all conditions up to those assumed in the accident analyses presented in Chapter 13.
- 2. Chemical, thermal, mechanical, and radiation compatibility within VIPR core environment.

Moderation of fission neutrons to thermal energies is accomplished by the light water coolant circulated through the fuel pins in the heterogeneous core and the heavy water contained in the adjacent DANK tank. To a lesser degree, the coolant present in the pool in which the core is submerged and the beryllium neutron reflector in the center of the core provide further neutron moderation.

4.2.3.1 Primary Coolant

The fuel geometry, including pin diameter and pitch, and VIPR operating technical specifications, including coolant temperature and pressure (specified in Chapter 14), result in a core that is undermoderated. As the primary moderator is the coolant, any increases in reactor power produce a corresponding increase in moderator temperature and decrease in moderator density. Conversely, decreases in reactor power cause a decrease in moderator temperature and an increase in its density. In the under-moderated system, this implies a negative reactivity coefficient, and the VIPR is passively self-stabilizing and resistant to power excursions.

Forced convection of light water through the core is provided by the pumps of the Primary Coolant System (PCS), while coolant chemistry and inventory are maintained by the Chemical and Volume Control System.



AAI-PSAR-04 (NP) Rev 0 Page 4-20

Several nuclear reactions can occur in the coolant as it passes through the core and is exposed to the high radiation flux:

•
$${}_{1}^{1}H_{0} + n \rightarrow {}_{1}^{2}H_{1}$$

Radiative capture of thermal neutrons in the hydrogen comprising the majority of the light water produces stable deuterium. The low natural abundance of deuterium results in this reaction becoming the primary source of the isotope in the moderator. Produced deuterium will not significantly alter the cooling, moderating, mechanical, or chemical properties of the material.

•
$${}_{1}^{2}H_{1} + n \rightarrow {}_{1}^{3}H_{2}$$

Produced deuterium can capture an additional neutron and create radioactive tritium. Because the reaction requires deuterium, the majority of which will be produced artificially in the moderator, the quantity of tritium produced will not require special cleanup systems. Produced tritium will not significantly alter the cooling, moderating, mechanical, or chemical properties of the material. Nonetheless, tritium levels will be routinely monitored in the reactor pool and the atmosphere of the building.

•
$${}^{16}_{8}O_{8} + n \rightarrow p + {}^{16}_{7}N_{9} \xrightarrow{T_{1/2} = 7.16 \, s} \beta^{-} + {}^{16}_{8}O_{8}$$

Oxygen-16 (O-16) in the light water can be transmuted by high energy neutrons into radioactive nitrogen-16 (N-16). Because the reaction occurs at high neutron energies, N-16 will only be produced within or in very close proximity to the core. The reaction disassociates the water molecule to produce hydrogen, nitrogen, and, after the N-16 decays, oxygen gases. N-16 poses a radiation hazard; the mitigation of the radioactive isotope is discussed in Chapter 5. The accumulation and mitigation of combustible hydrogen and oxygen gasses is also discussed in Chapter 9. The destruction of moderator material by this reaction is negligible compared to other removal or destruction mechanisms (e.g. evaporation) which will be mitigated by the chemical and volume control system. This process will not significantly alter the cooling, moderating, mechanical, or chemical properties of the material.

Further discussion of the VIPR coolant is given in Section 4.6.

4.2.3.2 **DANK Tank**

Reflection of neutrons back into the fuel region of the VIPR is provided by the DANK tank radially surrounding the VIPR core. The heavy water provides moderation of neutrons for utilization in the fuel as well as core-adjacent irradiation facilities. The tank is cylindrical with a square void in the center housing the reactor and containing the flow of primary coolant through the fuel region, shown in **Figure 4-1**. The VIPR irradiation facilities are contained in penetrations through the reflector, primarily along the inner surface adjacent to the core but also near the outer cylindrical tank wall, that are open to the light water coolant contained in the reactor pool. Additional detail, including geometrical dimensions, are provided in Figure 10-4 in Chapter 10, "Experimental Facilities and Utilization."

The system provides an alternate and redundant means of rapidly shutting down the reactor. Heavy water may be drained from the DANK tank, introducing a void around the core and enough negative reactivity to render the core subcritical in combination with a subset of the control rod assemblies.



AAI-PSAR-04 (NP) Rev 0 Page 4-21

The auxiliary systems are described in further detail in Chapter 9 with the instrumentation and control of said systems outlined in Chapter 7.

The DANK tank is mechanically fastened to a support structure installed on the liner of the bottom of the reactor pool and independent of the core support structure. All surfaces in contact with the heavy water in the tank are either stainless steel, rubber, or aluminum. All free surfaces within the tank are blanketed with a helium cover gas.

Due to the presence of deuterium as the principal constituent of the heavy water in the reflector adjacent to the core, the same tritium-producing neutron capture reaction occurring in the light water coolant occurs at a greater rate. Owing to the long half-life of the isotope, tritium activity in the heavy water is predicted to increase without bound; a tritium cleanup system is necessary for containment and maintenance of the isotope at acceptable concentrations is described in Chapter 9.

4.2.3.3 Beryllium Neutron Reflector

Additional moderation and reflection of neutrons back into the fuel region is provided by the beryllium reflector located at the center of the VIPR core. The reflector is a square cuboid, having equal length and width, composed of beryllium metal with [] PROP,ECI cylindrical channels machined through its height. The location of the reflector is shown in **Figure 4-6**. The channels are open to the light water pool and facilitate the online insertion and removal of irradiation targets from the VIPR. The size and location of the channels within the beryllium reflector are chosen to maximize the thermal neutron flux within irradiation targets installed in the channels.

The beryllium reflector is mechanically fastened to the core support structure, allowing for its replacement as needed, including the potential of radiation-induced swelling.

Several nuclear reactions can occur in the beryllium reflector as it is exposed to the high radiation flux:

•
$${}^{9}_{4}Be_{5} + n \rightarrow \alpha + {}^{6}_{2}He_{4} \xrightarrow{\frac{T_{1}}{2} = 0.81 \, s} {}^{6}_{3}Li_{3} + n \rightarrow \alpha + {}^{3}_{1}H_{2}$$

Tritium is produced in the beryllium reflectors in significant quantities by a two-step radiative capture reaction beginning with the isotopically abundant beryllium-9 (Be-9), producing in total two alpha particles and one tritium nucleus.

•
$${}^{9}_{4}Be_{5} + n \ (> 2 \ MeV) \rightarrow 2\alpha + 2n$$

•
$${}^9_4Be_5 + \gamma \ (> 1.67 \ MeV) \rightarrow 2\alpha + n$$

High energy neutrons and photons have small probabilities of destroying the Be-9 nucleus via fission or photofission, producing two alpha particles and ejecting the remaining reaction neutrons.

As a result of the primary nuclear reactions, as well as other minor reactions, the beryllium reflector experiences radiation-induced swelling and embrittlement over its lifetime, necessitating its replacement. This radiation damage in beryllium becomes significant at fast neutron fluences on the order of 10^{22} n/cm² depending on material grade and conditions. Based on estimated fast fluence accumulation in the VIPR reflector of neutron fluence on orders of 10^{14} n/cm² and analogous data from Oak Ridge National Laboratory's High Flux Isotope Reactor and Idaho National Laboratory's Advanced Test Reactor (where reflectors are replaced at similar fluence thresholds), replacement is anticipated



AAI-PSAR-04 (NP) Rev 0 Page 4-22

approximately every 15-20 years. Beryllium damage monitoring will follow this timeframe and this interval will be refined with fluence monitoring and inspection data. Neutron fluence limits specified in Chapter 14 of the FSAR will be used to determine the replacement intervals.

4.2.4 Neutron Startup Source

An americium-beryllium (AmBe) neutron source will be used for reactor startup as needed and for the testing of nuclear instrumentation. The AmBe neutron source will be located in one of the beryllium reflector irradiation positions inside of a standardized irradiation target container; when not in use, the startup source will be stored in a holder located in the reactor pool.

The geometry and activity of the AmBe neutron source will be provided in the FSAR.

4.2.5 Core Support Structure

The core support structure consists of a grid plate and plenum installed on the pool liner at the bottom of the pool. Fuel assemblies and the beryllium neutron reflector are installed on the core grid plate, with holes bored in a regular square array. The top of the coolant plenum serves as the grid plate that holds the fuel assemblies and beryllium reflector. No other systems and components, such as radiation shields or other experimental facilities are accommodated by the core support structure.

While the support structure itself is also subject to radiation effects, it's design accounts for anticipated volumetric swelling and associated mechanical stresses. The support will be fabricated from Type 316L stainless steel, a material with a proven record of performance in nuclear environments due to its high resistance to corrosion, irradiation damage, and mechanical degradation.

To further mitigate swelling and creep, the material will undergo controlled processing methods intended to produce a fine-grained microstructure and increased dislocation density, consistent with industry best practices for radiation-exposed core structures. The resulting metallurgical condition improves the material's dimensional stability and long-term structural integrity under neutron irradiation.

The support structure is specifically designed to maintain uniform surface elevation and resist differential distortion, ensuring consistent vertical positioning of both the central reflector and the surrounding fuel assemblies. Radial and vertical tolerances are maintained to preserve clearances, alignment, and load-bearing integrity under expected irradiation and thermal conditions.

The support structure is designed to provide stable mechanical performance. However, its configuration permits future replacement during scheduled maintenance activities, should inspection data or operating experience indicate significant degradation. This approach ensures long-term dimensional stability and preserves radial and vertical tolerances without committing to premature or unnecessary replacement. The design philosophy reflects the expected radiation tolerance of coldworked Type 316L stainless steel under the reactor's operational fluence and thermal conditions.

The core support structure will be designed to hold the weight of all core-related components and withstand all hydraulic, mechanical, chemical, and radiation stresses to which it is subjected. A preliminary design of the core support structure is shown in **Figure 4-14**. The structure, constructed of 316L stainless steel, is designed to withstand 14.2 kN of force from core components; models of static mechanical stress and displacement are shown in **Figure 4-15** and **Figure 4-16**, respectively. While



AAI-PSAR-04 (NP) Rev 0 Page 4-23

further detail is also described in section 4.2.3.3 above regarding plenum structural performance. A detailed description of the core support structure will be provided in the FSAR.

[]PROP,ECI

Figure 4-14: Isometric rendering of the core support structure



AAI-PSAR-04 (NP) Rev 0 Page 4-24

[]PROP,ECI

Figure 4-15: Stress model of the core support structure



AAI-PSAR-04 (NP) Rev 0 Page 4-25

[PROP,ECI

Figure 4-16: Displacement model of the core support structure

4.3 REACTOR POOL

The VIPR is a pool-type reactor, installed in an open pool under [] PROP,ECI of high resistivity light water, with a total pool depth of [] PROP,ECI. The pool is cylindrical with diameter length of [] PROP,ECI. The total volume of pool structure is [] PROP,ECI, with the nominal volume of water contained being less due to the presence of the core, core support structure, primary coolant piping, DANK tank, tools, equipment, and irradiation targets. With the pool constructed of Type 304L stainless steel plate of thickness 0.635 cm (3 gauge) with stiffener rings on the outside for additional support.

There are two penetrations made in the pool liner at an elevation of 4.8 m above the pool floor and near the pool floor to accommodate primary coolant piping: the penetration near the floor accommodates the primary coolant outlet, with the other accommodating the primary coolant inlet. A third penetration accommodates piping supporting the function of the heavy water neutron reflector system described in Section 4.2.3.2. The elevations of these penetrations provide the limiting conditions on pool depth utilized in the accident analyses discussed in Chapter 13.

Test coupons of pool liner material will be installed in the VIPR pool and periodically inspected for chemical damage, radiation-induced damage, and deterioration. While the pool is designed to last for



AAI-PSAR-04 (NP) Rev 0 Page 4-26

the full operational life of the reactor, provisions exist to address any localized damage that may occur. Routine monitoring of water chemistry – particularly pH level and conductivity – along with regular inspections for signs of corrosion or stress corrosion cracking, will support long term material integrity. If localized corrosion or damage is detected, in situ repair methods, such as robotic welding, can be employed. These preventive and corrective measures collectively help ensure the longevity and continued performance of the pool structure.

4.4 BIOLOGICAL SHIELDING

The biological shield consists of the light water within the pool, the heavy water within the DANK tank,
and the concrete surrounding the pool. The total depth of the reactor pool is [] PROP,ECI; the core
support structure raises the height of the VIPR significantly above the bottom of the pool, resulting in a
depth of []PROP,ECI of light water above the core. The shielding at the level of the core consists of,
at minimum, []PROP,ECI of light and heavy water, and []PROP,ECI of high-density barytes
concrete as the outer boundary. The baryte concrete reduces more radiation than regular concrete
can, maintains structural performance under high radiation, and because of the higher density it allows
for thinner concrete. It has also a long history of proven performance in nuclear facilities. At several
elevations above the core, where the radiation flux is increasingly reduced by the depth of the water,
the thickness of the concrete shielding is also reduced. Irradiation and activation of the groundwater
and soils surrounding the reactor shield is prevented by a concrete foundation of sufficient thickness to
prevent neutron activation of the soil underneath. Isometric renderings of the biological shield are
shown in Figure 4-17 and Figure 4-18.

Depending on the region and elevation, thickness of the high-density concrete varies. The thicknesses on the side abutting the pit containing the heat exchangers and pumps are:

- []PROP,ECI thick concrete pad forming the bottom of the reactor pool and basement floor
- []PROP,ECI thick from the basement floor to a height of []PROP,ECI
- []PROP,ECI thick from []PROP,ECI to []PROP,ECI

The thicknesses on the side adjacent to the transfer canal are:

- []PROP,ECI thick concrete pad forming the bottom of the reactor pool and basement floor
- []PROP,ECI thick from the basement floor to a height of []PROP,ECI

The thicknesses on the two sides of the biological shield between the pit and canal are arranged in tiers as follows:

- []PROP,ECI thick concrete pad forming the bottom of the reactor pool and basement floor
- [] PROP,ECI thick from the basement floor to a height of [] PROP,ECI
- []PROP,ECI thick from []PROP,ECI to []PROP,ECI
- []PROP,ECI thick from []PROP,ECI to []PROP,ECI

Isometric renderings of the biological shield are shown in **Figure 4-17** and **Figure 4-18**. The concrete thicknesses are derived from criteria relating to its role as a biological shield as described in Section 4.4; preliminary simulations have shown that the structure easily withstands anticipated mechanical stresses.



AAI-PSAR-04 (NP) Rev 0 Page 4-27

[PROP,ECI

Figure 4-17: Transfer canal-side isometric view of the biological baryte shielding



AAI-PSAR-04 (NP) Rev 0 Page 4-28

[PROP,ECI

Figure 4-18: Auxiliary pit-side isometric view of the biological baryte shielding

Neutron and gamma-ray fluxes at various locations around the biological shield were determined through Monte Carlo simulation in MCNP 6.2.

Source terms included in the simulations are the fuel in the VIPR core, materials in and around the core which may produce secondary radiations in the high radiation environment, and Mo-99 production targets in the appropriate irradiation positions in the DANK tank. The model was run as a criticality calculation to replicate the spatial and energy distributions of fission neutrons, photons, and secondary radiations.

Variance reduction techniques, particularly mesh-based weight windows, were used to obtain adequate statistics in the low flux regions outside of the biological shield. Tally results were normalized according to the following scaling factor:

$$C = \frac{P\langle \nu \rangle}{\langle w_f \rangle k_{eff}}$$



AAI-PSAR-04 (NP) Rev 0 Page 4-29

where the normalization constant is a function of the reactor power P, the average number of neutrons produced per fission ν , the average recoverable energy released per fission w_f , and the effective neutron multiplication factor k_{eff} . Values used in the calculation of the normalization coefficient were 16 MWth, 2.455 neutrons per fission, 190.3 MeV per fission, and 1.00397, respectively. The average number of neutrons produced per fission and effective neutron multiplication factor were obtained from the MCNP results, while the average recoverable energy released per fission was obtained from the ENDF/B-VIII.0 library for U-235.

Dose rates were determined through the implementation of energy-dependent fluence-to-dose conversion coefficients provided in ANSI/ANS-6.1.1-2020. Different coefficients for each particle at each energy are provided for different bodily orientations; the maximum coefficient among the various orientations at each energy was chosen to calculate a bounding dose rate.

The total dose rates at locations of significance around the reactor pool are described in **Table** 4-4. The locations where dose rates were estimated are shown on XZ and YZ cross sections of the VIPR, reactor pool, and shielding depicted in **Figure 4-19**. The numbered locations correspond to areas at which dose rates were estimated. Materials of significance in the dose rate simulations, specifically the primary coolant in the reactor pool, biological shield concrete, and earth surrounding the reactor pool, are colored in blue, gray, and brown, respectively.

Table 4-4: Total dose rates around the reactor pool

Location	Dose Rate (mrem/hr)	
Pool Surface	[]PROP,ECI Pool Depth (1)	0.0266
1 oor surrace	[]PROP,ECI Pool Depth (2)	0.3326
	Core Height, Outer Surface of Biological Shield (3)	2.8543
Basement	On First Tier, Corner Closest to Core (4)	0.2412
	On Second Tier, Corner Closest to Core (5)	0.0002
Primary Bay	Corner Closest to Core (6)	0.0409



AAI-PSAR-04 (NP) Rev 0 Page 4-30

ſ

PROP,EC

Figure 4-19: XZ and YZ cross sections of the VIPR pool and shielding.

No neutron flux was recorded at any occupied location outside of the biological shield; dose rates are the result of photon flux only.

At the nominal pool level, adequate shielding is provided by the depth of water such that additional shielding is not required above the core. The pool is deep enough that any reductions in the pool level, whether by evaporation or leakage, will not significantly increase the expected radioactive dose before pool level alarms sound. Radioactive N-16 produced by neutron activation in the water contributes a significant dose at the pool surface and is reduced by the N-16 suppression system installed above the core, described in Chapter 9.

4.5 NUCLEAR DESIGN

4.5.1 Normal Operating Conditions

4.5.1.1 Core Components

The VIPR core has no fewer than nine components installed on the grid plate, comprised of [] PROP,ECI fuel assemblies with installed control rod assemblies, [] PROP,ECI fuel assembly with an installed regulating rod assembly, [] PROP,ECI fuel assemblies with no installed control elements, and one neutron reflector. By administrative control and mechanical design, no core components may be installed in locations other than those intended for that type of component. No vacancies are allowed in the positions designated for the fuel assemblies and reflector, ensuring a compact core in all planned configurations.



AAI-PSAR-04 (NP) Rev 0 Page 4-31

The DANK tank support structure may be extended beyond the tank to accommodate external experiment racks and target irradiation facilities.

4.5.1.2 Core Configurations

Two distinct core configurations are planned during the life of the VIPR, differentiated by the degree of fuel burnup and fission product accumulation in the fuel assemblies.

- 1. The initial core fuel loading comprised entirely of new fuel assemblies. This core configuration is the "limiting" core configuration which produces the greatest power densities and fuel temperatures and is the reactor state utilized in the accident analyses provided in Chapter 13.
- 2. All subsequent core fuel loadings consist of a mix of new and reshuffled fuel assemblies. The VIPR is operated such that the fuel is depleted and reshuffled to maintain configurations similar in quantity and spatial distribution of fuel and poisons, including fission products, activation products, and those added by design. This configuration is considered the "steady state" core configuration.

Core configurations are differentiated only by the number of new fuel assemblies installed. The location of all other core components remains unchanged, ensuring a compact core in each configuration.

Each fuel assembly is shuffled once during its residence in the core: fresh fuel assemblies are initially loaded in the corner positions, moved to the positions adjacent to the central reflector after one operating cycle, and finally discharged following a second operating cycle.

The limiting core configuration has sufficient excess reactivity to operate for over [] PROP continuous days at 15 MWth. Operating the first VIPR core until all excess reactivity is depleted produces burnups in excess of the steady state configuration in the corner fuel assemblies, which are shuffled into the second fuel loading. This results in less excess reactivity at the start of the second operating cycle and a shorter cycle length, leading to decreased burnup, increased excess reactivity, and a longer third fuel cycle. The excess reactivities and cycle lengths oscillate in this manner until converging at the steady state configuration after an undetermined number of fuel cycles. This behavior is avoided by ending the initial fuel cycle prematurely to avoid excessive depletion in the fuel assemblies to be reshuffled in the next operating cycle and enable the transition into the steady state core configuration. Simulations in Serpent 2 (Serpent) show the magnitude and distribution of pin-wise burnup in the corner fuel assemblies at the end of the steady state fuel cycle is most similar to [] PROP days of full power operation in the initial fuel cycle. Ending the initial fuel cycle at this point results in the second fuel cycle, and all following fuel cycles, having the characteristics of the steady state configuration.

Data describing the characteristics of the limiting and steady state configurations are given in **Table** 4-5. **Figure 4-20** shows the time-dependent excess reactivity in each configuration; it should be noted that while the effects of the power defect are accounted for by simulating the VIPR in a cold condition, the negative worth from fission product poisons is still present. Taking this into account by adding the appropriate value from **Table** 4-3, the maximum excess reactivity of [] PROP,ECI pcm in the limiting configuration occurs at 255 days.



AAI-PSAR-04 (NP) Rev 0

Page 4-32

Table 4-5: Core configuration reactivity characteristics

Parameter	Limiting Configuration	Steady State Configuration
Excess Reactivity, Startup (pcm)	7,855	7,831
Cycle Length (d)	[]PROP,ECI	[]PROP,ECI
Reactivity Consumption (pcm/MWd)	0.31	0.93

[]PROP,ECI

Figure 4-20: Fuel cycle excess reactivity in limiting and steady state configurations

1^{PROP,ECI} pcm of excess reactivity is consumed, Over the length of the first operating cycle a net [lPROP,ECI pcm/MWd. The rate of reactivity yielding an average reactivity consumption rate of [consumption changes throughout the cycle and is influenced by a number of factors, including the production of fission product poisons, the depletion of burnable poisons, the net reactivity of targets irradiated throughout the cycle, and depletion of the fuel. Following an initial decrease as fission product neutron poisons, particularly Xenon-135 (Xe-135) and Samarium-149 (Sm-149), build to their equilibrium concentrations, the excess reactivity of the system increases due to the removal of the burnable poisons.]^{PROP}, assuming continuous The length of the steady state operating cycle is approximately [1 PROP,ECI pcm of excess reactivity is consumed, yielding an average operation at 15 MWth. A net []PROP, ECI pcm/MWd. The rate of reactivity consumption is reactivity consumption rate of [approximately constant throughout the cycle apart from the initial rapid decrease in reactivity as Xe-



AAI-PSAR-04 (NP) Rev 0 Page 4-33

135 and Sm-149 build to their equilibrium concentrations. Further discussion of the steady state operating cycle will be provided in the FSAR.

Each fuel assembly spends approximately [] PROP in the VIPR core and achieves a maximum burnup of approximately [] PROP,ECI GWd/MTU before it is discharged. The length of the VIPR cycle is consequently limited by the available excess reactivity rather than by limits on the burnup of the fuel.

Installation of new fuel assemblies in the corner positions ensures that the cycle length is determined primarily by the excess reactivity contained in the depleted assemblies located in the higher worth positions adjacent to the central reflector and that the burnup in these assemblies is maximized. This shuffling pattern has the added advantage of shifting the power distribution away from the inner edges of the side assemblies out towards the corner assemblies, flattening the power distribution and reducing peaking. The geometrical effects contributing to the large integral worth of the control rod assemblies described in Section 4.2.2 remain in the refueled VIPR core.

4.5.2 Reactor Core Physics Parameters

Reactor core physics parameters are generally determined through stochastic simulation in the Serpent model of the VIPR. Sufficient particle histories are tracked to ensure statistical errors in the reported values are less than 1%. In simulations involving power distributions throughout the VIPR core, the rate at which histories are recorded in some low power regions of the core is so low as to make uncertainties under 1% unachievable in a reasonable time. In these cases, uncertainties are generally under 10%; this was determined to be acceptable because of the relatively low power of these regions and their correspondingly small impact on the core physics as a whole.

The results of verification and validation of Serpent against other neutron transport codes and experimental data are provided in the Serpent 2 user manual. Atomic Alchemy followed the installation process specified in the Serpent 2 user manual.

4.5.2.1 Neutron Lifetime and Delayed Neutron Fraction

Over the course of the initial limiting fuel cycle the effective delayed neutron fraction of the core is predicted to decrease from 0.66% to 0.60% as U-235 is depleted and Pu-239 is produced. The delayed neutron fraction increases again to 0.63% at the start of the steady state fuel cycle, when the VIPR is refueled, followed by a decrease to 0.60%. These values are estimated from the Serpent model of the VIPR, which approximates β_{eff} as the fraction of fissions caused by delayed neutrons. The total delayed neutron and group fractions and precursor decay constants are provided in **Table** 4-6 and **Table** 4-7.

Table 4-6: Delayed neutron fractions (β) and decay constants (λ) for the limiting configuration

	Limiting Configuration, Cycle Start		Limiting Configuration, Cycle End	
	β	λ (s ⁻¹)	β	λ (s ⁻¹)
Total	6.55E-03	4.93E-01	6.04E-03	4.90E-01
Group 1	2.23E-04	1.22E-02	1.93E-04	1.18E-02
Group 2	1.12E-03	3.26E-02	1.07E-03	3.24E-02
Group 3	1.08E-03	1.21E-01	1.01E-03	1.21E-01

AAI-PSAR-04 (NP) Rev 0 Page 4-34

	Limiting Configuration, Cycle Start		Limiting Configuration, Cycle End	
Group 4	2.53E-03	3.05E-01	2.31E-03	3.05E-01
Group 5	1.15E-03	8.59E-01	1.05E-03	8.60E-01
Group 6	4.51E-04	2.85E+00	4.18E-04	2.84E+00

Table 4-7: Delayed neutron fractions (β) and decay constants (λ) for the steady state configuration

	Steady State Configuration, Cycle Start		Steady State Configuration, Cycle End	
	β	λ (s ⁻¹)	β	λ (s ⁻¹)
Total	6.29E-03	4.90E-01	6.02E-03	4.91E-01
Group 1	2.21E-04	1.17E-02	1.75E-04	1.07E-02
Group 2	1.06E-03	3.25E-02	1.05E-03	3.24E-02
Group 3	1.06E-03	1.21E-01	1.03E-03	1.20E-01
Group 4	2.44E-03	3.05E-01	2.32E-03	3.05E-01
Group 5	1.08E-03	8.60E-01	1.03E-03	8.63E-01
Group 6	4.30E-04	2.85E+00	4.15E-04	2.88E+00

The total neutron lifetimes, as well as its prompt and delayed neutron components, at the start and end of the limiting and steady state cycles are provided in **Table** 4-8 and **Table** 4-9, respectively.

Table 4-8: Total, prompt, and delayed neutron lifetimes for the limiting cycle

	Limiting Configuration, Cycle Start	Limiting Configuration, Cycle End
Total Lifetime (s)	6.35E-05	6.35E-05
Prompt Lifetime (s)	6.36E-05	6.36E-05
Delayed Lifetime (s)	5.40E-05	5.15E-05

Table 4-9: Total, prompt, and delayed neutron lifetimes for the steady state cycle

	Steady State Configuration, Cycle Start	Steady State Configuration, Cycle End
Total Lifetime (s)	6.33E-05	6.57E-05
Prompt Lifetime (s)	6.33E-05	6.57E-05
Delayed Lifetime (s)	6.46E-05	5.61E-05



AAI-PSAR-04 (NP) Rev 0 Page 4-35

4.5.2.2 Reactivity Coefficients

Temperature effects manifest in inherent features of the VIPR design that passively oppose power changes and acts to correct minor deviations of the reactor system from criticality. The primary temperature effects present in the VIPR are resonance absorption of neutrons by U-238, thermal expansion of the light water coolant, and the formation of voids in the light water coolant.

As the temperature of the fuel increases the U-238 resonance absorption peaks widen, making the absorption of neutrons at those energies more probable. Because the VIPR relies on thermal neutron fissions in U-235 to maintain criticality, the capture of epithermal neutrons before they can be moderated to thermal energies decreases the reactivity of the system. Conversely, decreasing fuel temperatures causes resonance absorption to decrease and increases the reactivity of the system.

Temperature changes in the coolant also oppose power changes, albeit by a different mechanism. When the temperature of the coolant increases following a positive power change, the coolant expands and becomes less dense. Because the VIPR is designed to be under-moderated, a less dense coolant effectively removes moderator from the core and causes the VIPR to become increasingly under-moderated, which lowers reactivity. The opposite effect occurs when power is decreased and the coolant contracts.

While the magnitude of the response of the reactor to a temperature change in the fuel is less than that of the same temperature change in the coolant, feedback effects in the fuel are more significant for two reasons. First, the temperature of the fuel changes nearly instantly in response to power increases as compared to the coolant, which is delayed in its temperature response by the low thermal conductivity of the ceramic fuel and the intermediate layers between it and the coolant. Second, although the reactivity change per unit temperature of the fuel is lower than that of the coolant, the total reactivity change is greatest in the fuel because of the larger range of temperatures present in the material. The VIPR is designed to avoid bulk boiling of the coolant, limiting its maximum temperature to its boiling temperature close to 100°C; the ceramic fuel can experience temperatures in excess of 2000°C during normal operations.

While the VIPR has been designed to avoid bulk boiling of the coolant, localized nucleate boiling is expected to occur. With the coolant in the core taken as a whole, the introduction of relative voids in the coolant through boiling represents an effective decrease in the density of the coolant. Because the VIPR is designed to be under-moderated, the effective removal of coolant from the core resulting from increasing reactor power works to oppose the power change and stabilizes the criticality of the system. Because both the rate of localized boiling and thermal expansion of the coolant are correlated with the temperature of the coolant, void effects are an additional component of the overall temperature effect in the coolant.

Reactivity coefficients were quantified and their signs determined by simulation of the VIPR core at the beginning of the first fuel cycle in Serpent. Each effect was analyzed in the following ways:

• Fuel Temperature Coefficient



AAI-PSAR-04 (NP) Rev 0 Page 4-36

The temperature of the fuel material was adjusted to a number of points between the core coolant inlet temperature and the fuel melting temperature. The most appropriate cross section libraries were chosen for each temperature, then the data adjusted to the exact temperature by the Doppler-broadening preprocessor in Serpent. The simulation was run in criticality mode, with an effective neutron multiplication factor produced as the result.

• Moderator Temperature Coefficient

The temperature of the coolant material was adjusted to a number of points between the core coolant inlet temperature and its boiling temperature. The most appropriate cross section libraries were chosen for each temperature, including the thermal scattering data, then the data adjusted to the exact temperature by the Doppler-broadening preprocessor in Serpent. Coolant densities at each temperature were calculated according to **Equation** 4-4. The simulation was run in criticality mode, with an effective neutron multiplication factor produced as the result.

Moderator Void Coefficient

The density of the coolant material was adjusted to a number of points between its density at the core coolant inlet temperature and zero density. The simulation was run in criticality mode, with an effective neutron multiplication factor produced as the result.

The results of the reactivity coefficient analysis are provided in **Figure 4-21**, **Figure 4-22**, **Figure 4-23**, and **Table** 4-10.

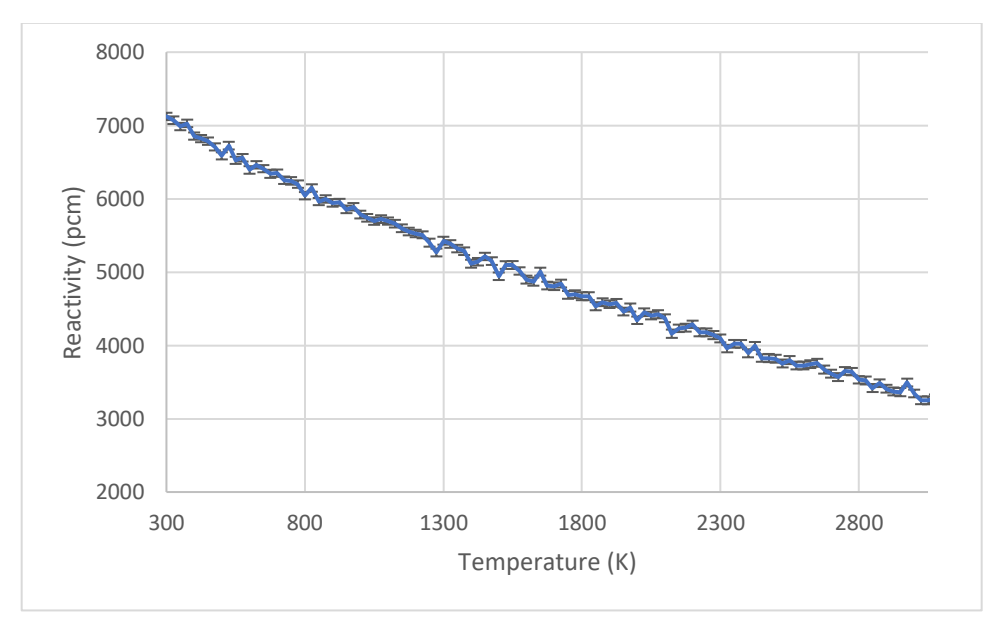


Figure 4-21: Reactivity change as a function of average fuel temperature



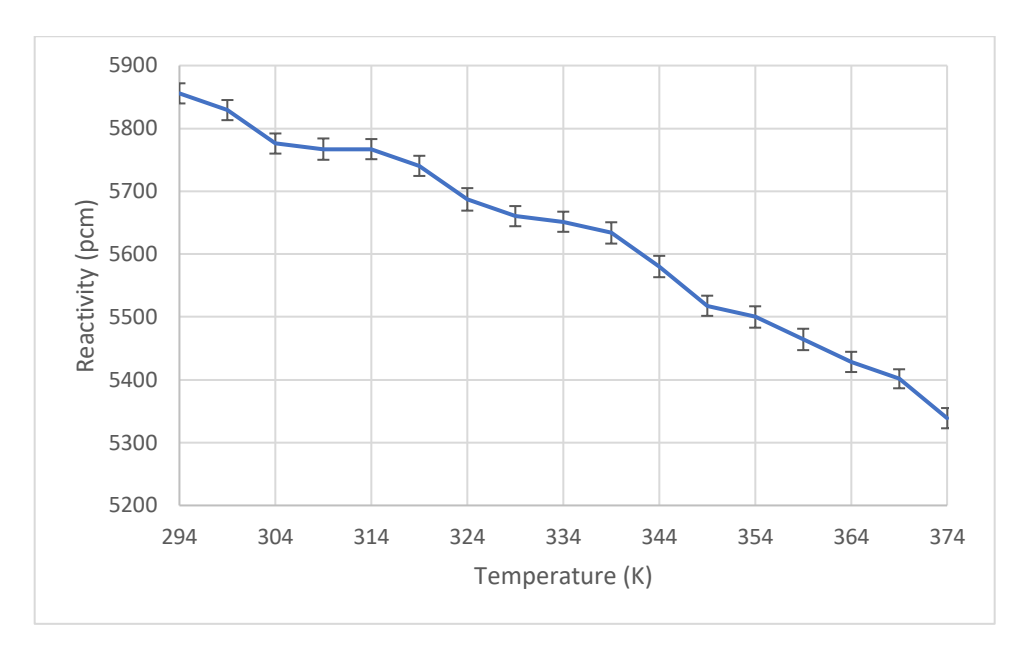


Figure 4-22: Reactivity change as a function of primary coolant temperature

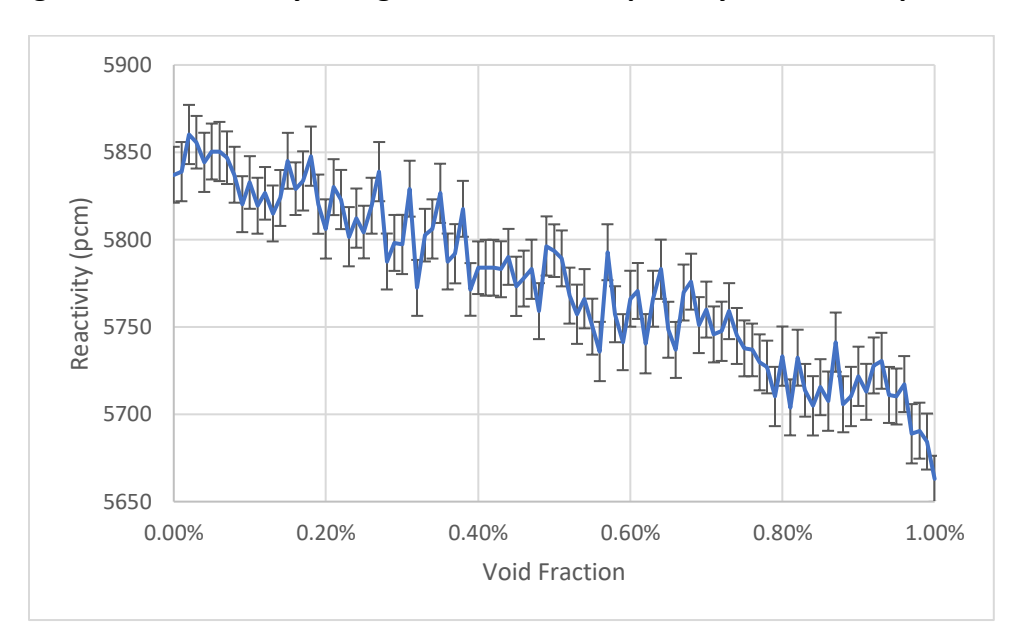


Figure 4-23: Reactivity change as a function of primary coolant void fraction

Table 4-10: Temperature-dependent reactivity coefficients at the beginning of the limiting cycle

Reactivity Coefficient	Value	Unit
Fuel Temperature	-1.35	pcm °C ⁻¹
Moderator Temperature	-6.09	pcm °C ⁻¹
Moderator Void	-153.61	pcm Δ% _{void} -1



AAI-PSAR-04 (NP) Rev 0 Page 4-38

The moderator void effect is given in void percentages of the entire core coolant volume; localized boiling will result in extremely small percentages on this scale, and correspondingly small reactivity changes.

The power defect of the VIPR is the change in the neutron multiplication factor or the total reactivity removed from the reactor through the process of bringing it from a cold shutdown condition to hot full power. The total negative reactivity added to the system between these two conditions is 1,174 pcm, determined as the difference in the neutron multiplication factor reported by Serpent from simulating the VIPR in both states. An additional 3,082 pcm of negative reactivity is added by the fission product poisons Xe-135 and Sm-149 at their equilibrium concentrations.

Reevaluation of these reactivity coefficients at other times in the limiting and steady state configurations has indicated that the magnitude of each effect decreases with increasing fuel burnup. However, sensitivity studies of the accident analyses described in Chapter 13 have shown that the power distribution, peaking factors, and maximal temperatures in the VIPR are most limiting in the response of the reactor and evolution of the discussed accidents. Consequently, the decrease in the magnitude of the reactivity feedback effects was determined to be less significant than the flattening of the power profile with increasing fuel burnup, and the most limiting condition in the operation of the VIPR remains at the start of the initial fuel cycle.

4.5.2.3 Power Distribution

Radial and axial power distributions were obtained through stochastic simulation of the VIPR core in Serpent. Input parameters used to calculate temperature and density distributions in Serpent power distribution simulations are shown in **Table** 4-11. A cartesian mesh detector was used to obtain the total fission power produced within axial bins spanning the height of every fuel pin in the reactor and produce a three-dimensional power distribution across the VIPR core. The predicted power distribution was used in external fuel temperature, coolant temperature, and coolant density calculations to determine the corresponding temperature and density distributions. The following equations and parameters were used:

$$T_m(z) = T_0 + \sum_{n=0}^{z} \frac{q'_n}{mc_p}$$

Equation 4-1: Axial coolant temperatures as a function of fuel pin linear heat generation rate

$$T_f(z) = \frac{q'(z)}{2\pi} \left[\frac{1}{2k_f(T_f)} + \frac{1}{R_g h_g} + \frac{1}{k_c} ln \left(\frac{R_{co}}{R_{ci}} \right) + \frac{1}{R_{oo} \, k_o/\delta_o} + \frac{1}{R_{oo} h} \right] + T_m(z)$$

Equation 4-2: Axial fuel temperatures as a function of fuel pin linear heat generation rate



$$k_f = \begin{bmatrix} 1.31219 \times 10^{-1} \\ -2.23378 \times 10^{-4} T_f(z) \\ +2.03101 \times 10^{-7} T_f(z)^2 \\ -9.90270 \times 10^{-11} T_f(z)^3 \\ +2.47295 \times 10^{-14} T_f(z)^4 \\ -2.42534 \times 10^{-18} T_f(z)^5 \end{bmatrix}$$

Equation 4-3: UO₂ thermal conductivity fit

$$\rho_m = \begin{bmatrix} 9.99840 \times 10^2 \\ + 1.69452 \times 10^1 T_m(z) \\ - 7.98704 \times 10^{-3} T_m(z)^2 \\ - 4.61705 \times 10^{-5} T_m(z)^3 \\ + 1.05563 \times 10^{-7} T_m(z)^4 \\ - 2.80543 \times 10^{-10} T_m(z)^5 \end{bmatrix} \times [1 + 1.68979 \times 10^{-2} T_m(z)]^{-1}$$

Equation 4-4: Light water density fit

Table 4-11: Parameters used in the iterative calculation of the reactor's power, temperature, and density distributions

Symbol	Parameter	Unit
T_m	Coolant Temperature	°C
T_f	Fuel Centerline Temperature	°C
T_0	Coolant Inlet Temperature	°C
$ ho_m$	Coolant Density	g/cm ³
q'	Linear Heat Generation	W/cm
m	Coolant Mass Flow Rate	kg/s
c_p	Coolant Specific Heat Capacity	J/(g °C)
k_f	Fuel Thermal Conductivity	W/(cm °C)
R_g	Gap Mid-Radius	cm
h_g	Gap Conductance	W/(cm ² °C)
k_c	Cladding Thermal Conductivity	W/(cm °C)
R_{co}	Cladding Outer Radius	cm



AAI-PSAR-04 (NP) Rev 0 Page 4-40

Symbol	Parameter	Unit
R_{ci}	Cladding Inner Radius	cm
R_{oo}	Oxide Radius	cm
k_o	Oxide Thermal Conductivity	W/(cm °C)
δ_o	Oxide Thickness	cm
h	Cladding-Coolant Heat Transfer Coefficient	W/(cm ² °C)

Coolant density as a function of temperature was predicted by interpolating between data obtained from The National Institute of Standards and Technology (NIST) for the isobaric properties of light water at 202.65 kPa.

The temperature and density distributions were utilized in the Serpent simulation by means of the multi-physics interface file functionality. Specifically, the Type 2 multi-physics interface file format was used to import the distributions on an irregular cartesian mesh spanning the reactor pool and apply constant temperature and density values to the relevant materials within each three-dimensional bin. The power distributions were redetermined with the adjusted physical properties; power distribution simulations and external calculations were iterated until convergence was reached in all distributions.

A qualitative representation of the radial pin-wise distribution of power in the VIPR with higher and lower powers represented by red and white hues respectively is shown in **Figure 4-24**:



AAI-PSAR-04 (NP) Rev 0 Page 4-41

[PROP,ECI

Figure 4-24: Qualitative depiction of the VIPR pin-wise power distribution

The general trend in the radial power distribution is for the greatest fraction of the total reactor power to be produced in those pins closest to the center of the core, where the beryllium neutron reflector produces a high thermal neutron flux. The pin-wise power also increases near the reactor edges, particularly near the center of each face, due to the presence of the surrounding neutron reflector and proximity to the center of the core.

One notable deviation from the otherwise symmetrical radial distribution of the reactor power may occur with the use of the regulating rod cluster located in the northeast fuel assembly. Although the neutron-absorbing rods induce some power tilt when actuated through the VIPR core, the integral worth of the cluster is small compared to other sources of positive and negative reactivity in the reactor.

Due to the radial symmetry of the VIPR core, the hot pin, the fuel pin in the VIPR core which produces the greatest power at any axial location, can be located on the inner face of any of the [] PROP,ECI fuel assemblies directly adjacent to the center beryllium reflector. The powers produced within the five fuel pins closest to the center of each of the 4 inner faces is generally similar enough that stochastic uncertainties in the simulations. As a result, the identified hot pin can vary randomly among these 20 fuel pins across different simulations. The hot pin parameters used for various analyses is always taken from whichever fuel pin produces the greatest power at any axial location in a given simulation. Accounting for potential asymmetries in the VIPR core, such as the adjacent DANK tank, regulating

rods, and irradiation targets, causes small perturbations in the power distribution outside of the typical stochastic uncertainty of the simulation and leads to the more consistent selection of the hot pin.

The axial power in the VIPR fuel pins was calculated with a reactor power of 16.8 MWth and the maximum linear heat generation rate in the hot pin reduced to 472 W/cm. The result follows an approximately cosine shaped distribution with a peak that is biased towards the bottom of the core, as shown in **Figure 4-25**.

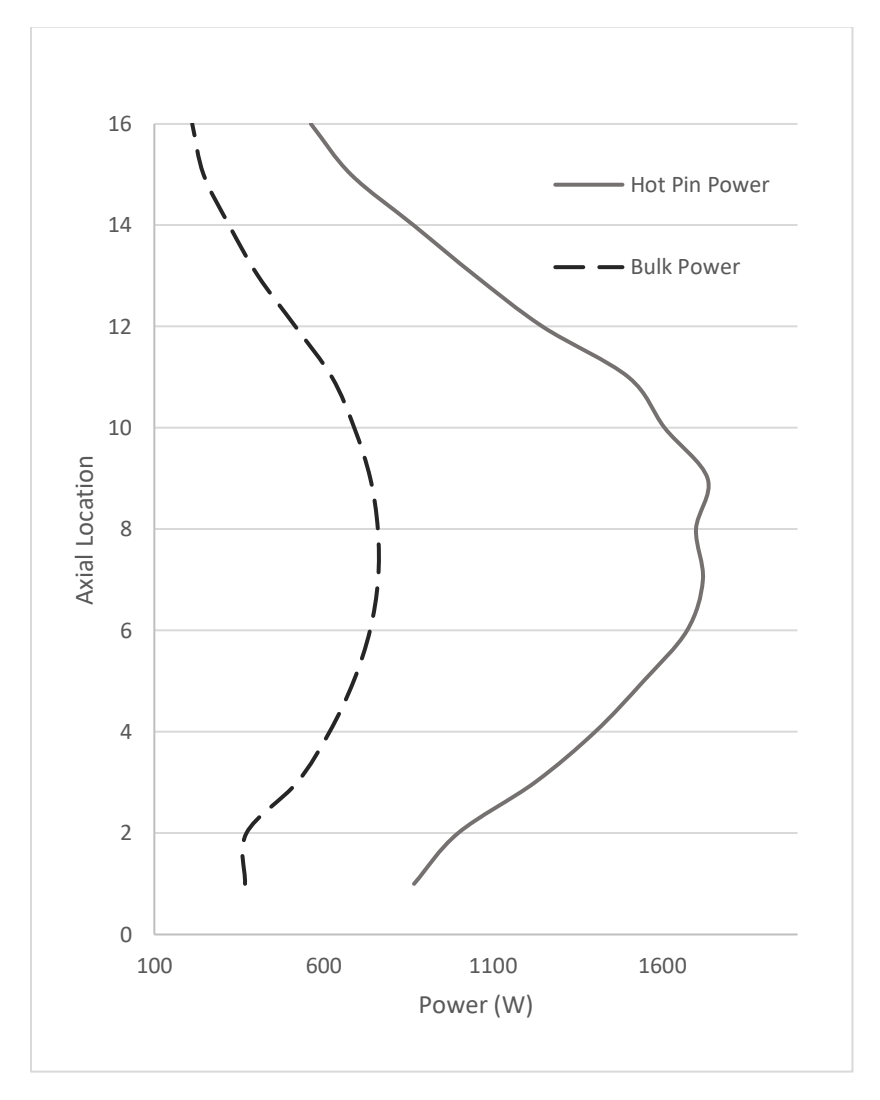


Figure 4-25: Axial power distribution in the hot pin and bulk fuel

4.5.3 **Operating Limits**

4.5.3.1 Reactivity Limits

Reactivity conditions and changes in reactivity over reactor operation are discussed in Section 4.5.1.2.



AAI-PSAR-04 (NP) Rev 0 Page 4-43

Limits on the maximum allowable excess reactivity under the "one stuck rod" criterion are discussed in Section 4.2.2. These limits ensure safe reactor operation, shutdown under any operating condition, and maintenance of the reactor in a safe shutdown state.

Transient analysis of the continuous ramp mode removal of the most reactive control rod from its most reactive region is considered in Chapter 13.

4.5.3.2 Limiting Core Configuration

Discussion of the limiting core configuration is given in Section 4.5.1.2. Safety limits and limiting safety system settings are derived from this core configuration.

4.6 THERMAL-HYDRAULIC DESIGN

4.6.1 <u>Design Criteria</u>

The VIPR thermal-hydraulic design consists of two modes of operation; forced convection and natural circulation. Forced convection cools the reactor during steady state operation up to 16.8 MWth. Natural circulation removes the decay heat from the reactor during shutdown conditions. The cooling of the VIPR core is based on the following design criteria to ensure that the fuel design bases described in Section 4.2.1 are met:

- Fuel temperature: The maximum fuel temperature will be maintained below 2600 °C.
- Cladding temperature: The maximum cladding temperature will be maintained below 1000 °C.
- Departure from nucleate boiling (DNBR): The DNBR will be higher than 2.0 for steady state conditions.
- Pool temperature: The maximum pool temperature will be maintained below 60 °C.
- Water height above the core: The depth of water above the core will be at least []PROP m during normal operation.

The design criteria are the premise for establishing the operating conditions that directly control the cooling capacity of the reactor core. The operating conditions are composed of interdependent variables for each mode of operation and are defined as follows:

Forced convection:

- Coolant mass flow rate
- Coolant subcooling in the core
- Reactor thermal power

Natural convection:

- Pool temperature
- Water height above the core
- Reactor thermal power

The combination of the design criteria and the interdependent variables derive the thermal-hydraulic core configurations in which the VIPR may operate:



AAI-PSAR-04 (NP) Rev 0 Page 4-44

4.6.1.1 Nominal Core Configuration

The intended operating conditions of the reactor core are presented in **Table** 4-12.

Table 4-12: Nominal interdependent variables for designed steady state operation

Variables	Value	Unit	
Reactor Thermal Power	15	MWth	
Mass Flow Rate	[]PROP	kg/s	
Mass Flow Hot Pin Subchannel	[]PROP	kg/s	
Coolant Temperature Inlet	[] ^{PROP}	°C	
Coolant Saturation Temperature	[]PROP	°C	
Pool Temperature	[]PROP	°C	
Water Height Above Core	[]PROP,ECI	m	

4.6.1.2 Limiting Core Configuration

The cooling capability in the nominal configuration is enveloped by the limiting core configuration, where the reactor operates at the lowest steady-state cooling capacity necessary to maintain the design criteria under all conditions up to and including any accident analyses described in Chapter 13.

The limiting core configuration is derived from the nominal values by establishing a range of operation. The large operating range of the power includes a 5% uncertainty in the instrumentation used to determine the reactor thermal power. The coolant system operating range incorporates instrumentation uncertainty and operational variances from the mechanical system described in Chapter 5. Any configuration of the four specified interdependent variables within the specified range in **Table** 4-13 will ensure there is sufficient cooling to the reactor core. The limiting configuration is the most extreme condition in which the reactor could operate during steady-state conditions and is the baseline for the calculations presented in this section and in Chapter 13.

Table 4-13: Reactor core parameters

Independent Variables	Minimal Values	Nominal Value	Maximum Values	Limiting Configuration	
Power (MWth)	-	15	16.8	16.8	
Mass Flow Rate (kg/s)	[]PROP	[]PROP	[]PROP	[]PROP	
Mass Flow Hot Pin Subchannel (kg/s)	[]PROP	[]PROP	[]PROP	[]PROP	
Reactor Coolant Temperature, Inlet (°C)	[]PROP	[]PROP	[]PROP	[] ^{PROP}	



AAI-PSAR-04 (NP) Rev 0 Page 4-45

Independent Variables	Minimal Values	Nominal Value	Maximum Values	Limiting Configuration	
Water Height Above Core (m)	[]PROP,ECI	[]PROP,ECI	[]PROP,ECI	[]PROP,ECI	

The limiting core configuration is presented in this section and is the set of initial conditions assumed in the accidents analyzed in Chapter 13. A complete parametric study will be done over the entire operating range specified in **Table** 4-13 in the FSAR. The lower subcooling and flow rate is considered the limiting configuration due to the decrease in heat transfer, corresponding to an increased probability of exceeding the critical heat flux (CHF) or the fluid reaching saturation temperatures and producing dynamic flow instabilities.

4.6.1.3 Fuel Characteristics

The thermal power density is derived from the neutron flux, which is dependent on the operating conditions of the reactor and converted to a linear heat generation rate to be used in the thermal-hydraulic analysis. The linear heat generation rate in the hot pin and bulk of the reactor core was determined from stochastic simulations in Serpent, utilizing temperature profiles calculated by RELAP5 Mod 3.3 (RELAP5). Power and temperature profiles were transferred iteratively between the codes until convergence was reached, to account for all thermal feedback effects in the limiting core and nominal core configurations.

The power density and maximum linear heat generation rate are greatest in a fresh core, immediately after startup with no fission product poisons present. The power distribution will flatten axially and radially with fuel burnup and the buildup of fission product poisons, reducing the peaking effect in the hot pin.

The safety analyses were performed using the limiting core configuration with a reactor power of 16.8 MW.

[

1PROP,ECI

4.6.1.3.1 Cladding Oxidation

The buildup of oxidation on the cladding surface is a common concern for the cooling of a fuel pin. Over the life of the fuel rod, exposure of the cladding surface to oxygen at an elevated temperature will cause a buildup of oxidation. The kinetics of the reaction are split into two regimes based on the corrosion rate. An analysis using the following correlations was done to determine the thickness of the oxidation layer on the fuel cladding over the life in the reactor core.



AAI-PSAR-04 (NP) Rev 0 Page 4-46

$$\frac{S^3}{dt} = K_{pre} \exp\left(\frac{-Q_{pre}}{RT_{co}}\right)$$

Equation 4-5: Pretransition oxidation layer thickness correlation

$$\frac{S}{dt} = K_{post} \exp\left(\frac{-Q_{post}}{RT_{co}}\right)$$

Equation 4-6: Post-transition oxidation layer thickness correlation

The coefficients used to determine the corrosion rate and potential oxidate impact on the fuel were taken from the Electric Power Research Institute (EPRI) (Pyecha, 1985) The results from the analysis indicate that the fuel at the end of the reactor cycle will form a 0.32 μ m thick oxide layer on the cladding surface. This indicates the oxidation will not surpass the pretransition corrosion boundary condition of 0.89 μ m using the boundary equation from EPRI (Pyecha, 1985) at a cladding surface temperature of 204°C.

The oxidation rate of the fuel was calculated for an additional 60 years of storage in the used fuel pool. At a cladding surface temperature of 50°C, the corrosion rate predicts an additional 0.004 μ m of oxidation on the cladding surface. The total 0.324 μ m oxidation thickness is well below the established limit for PWR fuel of 17% of the original cladding thickness.

The [] PROP,ECI cladding is subject to unique cladding corrosion equations and constants. The FSAR will provide full details on the corrosion rate using the proprietary corrosion correlations from [] PROP,ECI.

4.6.2 <u>Methodology</u>

The methods used to determine the temperatures and reactor core cooling capability were finite volume analysis for the coolant and a one-dimensional radial heat transfer equation for the fuel pins. The use of a one-dimensional radial heat transfer equation was justified because conduction in the radial direction is significantly higher than in the axial direction in the fuel pin. The heat transfer from the fuel pin surface was determined by both flow correlations and a two-phase correlation for both natural and forced convection.

4.6.2.1 Models

The software chosen to develop the heat transfer and cooling capability in the reactor core is the NRC-approved and distributed RELAP5 Mod 3.3. The code is used to calculate the temperatures, cladding to coolant heat transfer, and the two-phase boiling regime of the average reactor fuel pin and the hot fuel pin. The software also determines the heat flux, CHF, and DNBR to ensure sufficient cooling of all fuel pins. The code utilizes a finite volume method to balance the mass and energy transfer phenomena in the reactor and PCS. The code is designed with a large range of correlations for single and two-phase flow and heat transfer correlations to accommodate a large range of coolant conditions.



AAI-PSAR-04 (NP) Rev 0 Page 4-47

The verification and validation of the correlations implemented in RELAP5 has been documented extensively. Each release of RELAP5 undergoes extensive testing to ensure accurate predictions from the embedded correlations.

To ensure proper installation and functionality of the software, test cases are conducted and compared to standardized results, ensuring that the software will function as intended and the uncertainty is limited to the correlations used in the modeling. AAI followed the installation process specified in the RELAP5 user manual.

A range of different models were used to capture the thermal-hydraulics performance in the core and the PCS. The general model of the VIPR and PCS is detailed in the nodal diagram in **Figure 4-26.** The model includes the reactor, reactor pool, PCS, and secondary coolant system (SCS), and was used to determine how the SCS, pump operation, and valve control will impact the cooling of the core. The SCS is controlled through two control volumes and a time-dependent junction.

[



AAI-PSAR-04 (NP) Rev 0 Page 4-48

The model describing the cooling of the core for both forced and natural convection is detailed in **Figure 4-27**. The model only captures the reactor, reactor pool, building atmosphere, and the passive inlet ports for natural circulation. Time-dependent volumes and junctions were used to control the flow into the core and out of the reactor pool. Parametric studies of the different core configurations were done with this model due to the simple control of the time-dependent volumes and junction.

[PROP,ECI

Figure 4-27: RELAP5 nodal diagram of the VIPR core and pool

The core is separated into four regions based on the flow parameters and energy density. The nodal breakdown of these regions and their corresponding zones in the core is shown in **Figure 4-28**. This breakdown was done to provide details of the geometry-specific flow areas for each region and capture the performance of each zone to ensure all design criteria are met throughout the entire core. The flow areas captured in the detailed model are differentiated by the spacing between fuel assemblies and neutron reflectors.



AAI-PSAR-04 (NP) Rev 0 Page 4-49

[]PROP,ECI

Figure 4-28: RELAP5 detailed model of the VIPR core¹

The core volume and heat structure followed the nodalization guidelines from Volume 3 of the RELAP5 Mod 3.3 Manual for the number of axial volume nodes and radial heat structure nodes needed to ensure accurate modeling of the reactor. The top of the pool was held at atmospheric pressure with a control volume that represents the reactor confinement room in terms of volume, temperature, and pressure.

4.6.2.1.1 Heat Transfer Correlation

A radial conduction heat transfer equation was used to derive the temperature profile through a single fuel pin. This was done with the heat generated in the fuel pellet and conducted through the helium gap and the [] PROP,ECI cladding to the interface with the water. The primary point of interest was the heat transfer correlations used between the cladding surface and the coolant. Forced convection, natural convection and two-phase heat transfer correlations are used in the RELAP5. **Table** 4-14 describes the relation between the specific RELAP5 mode number, the heat transfer phenomenon, and the specific correlations used in the code.

_

¹ This mode is used in conjunction with the RELAP5 model diagrams depicted above in Figure 4-26 and Figure 4-27



AAI-PSAR-04 (NP) Rev 0 Page 4-50

rage 4-30

Table 4-14: Wall convection heat transfer mode numbers, reproduced from the RELAP5 manual

Mode Number	Heat Transfer Phenomenon	Correlations ²
0	Noncondensable Steam-Water	Kays, Dittus-Boelter , ESDU, Shah, Churchill-Chu, McAdams
1	Supercritical or Single-Phase Liquid	Kays, Dittus-Boelter , ESDU, Shah, Churchill-Chu, McAdams
2	Single-Phase Liquid or Subcooled Wall with Voidg < 0.1	Kays, Dittus-Boelter , ESDU, Shah, Churchill-Chu, McAdams
3	Subcooled Nucleate Boiling	Chen
4	Saturated Nucleate Boiling	Chen
5	Subcooled Transition Boiling	Chen-Sundaram-Ozkaynak
6	Saturated Transition Boiling	Chen-Sundaram-Ozkaynak
7	Subcooled Film Boiling	Bromely, Sun-Gonzales, and Mode 0 Correlations
8	Saturated Film Boiling	Bromely, Sun-Gonzales, and Mode 0 Correlations

The heat transfer correlations used in the code are dependent on the coolant flow characteristics. The software calculates the natural, laminar, or turbulent convection heat transfer. The design of the core requires the use of forced convection during steady state operation and natural convection during shutdown conditions. A range of correlations were used depending on the state of the reactor.

The list of correlations available for use in heat transfer modes 0-2 in **Table** 4-14 requires identification of the correlations used in the model. The turbulent forced convection correlation used in the model was dependent on the flow field or the hydraulic geometry. For a vertical fuel pin bundle with cross flow, the Dittus-Boelter-Inayat-Shah correlation (Shah 1992) is used for improved modeling of shell and tube heat exchangers and to incorporate mixing parameters in the core. The correlations used in the RELAP5 modeling for natural convection were the Churchill-Chu correlations. The DNBR was calculated by using the critical heat flux from the Groeneveld lookup tables. A correction factor of 0.8 was applied to the CHF value to adjust for the different tube geometry used to obtain the experimental data in the Groeneveld lookup tables.

4.6.2.2 Uncertainty

The preliminary design of the PCS and its cooling capability produced large safety margins to compensate for uncertainties in operating parameters and instrumentation and to ensure that, upon

² Complete references corresponding to the names listed in the Correlations column can be found in the Reference section.



AAI-PSAR-04 (NP) Rev 0 Page 4-51

final design, the reactor will be sufficiently cooled within operating and safety limits. To ensure that proper safety margins for the cooling capacity of the reactor were met, the uncertainty and accuracy of the correlations used in modeling were evaluated.

AAI considered the following uncertainties in the thermal-hydraulic analysis:

- Material Properties: Temperature dependent properties of the fuel, reflectors, and coolant were used in all models. The thermal properties and their errors for the fuel pins, reflectors, and water were considered in the thermal-hydraulic analysis results.
- **Size Tolerances:** The flow area through the core was calculated with nominal values. This analysis will consider size tolerances in the FSAR once details on the tolerances of the fuel and grid spacers are provided by []PROP,ECI.
- **Correlations:** Each correlation used to determine the heat transfer coefficient and resulting heat flux was subject to the uncertainty analysis to determine the cooling capacity of the reactor core. The design and safety margin of the cooling capability is sufficiently large enough to envelope the uncertainty of the correlations. Limiting the minimal DNBR to 2.0 for all steady state operating conditions bounded the uncertainty of the heat transfer correlations used in the RELAP5 analysis.
- Instrumentation: The error estimated from uncertainties in the instrumentation used in
 monitoring the conditions of the facility, as well as the margin of operation in the pumps and
 control systems, was considered in the design of the facility. The specific margin of error for the
 instrumentation and the operating variation in the pumps and control systems will be specified
 in the FSAR once the final design is completed.

4.6.3 Steady-State Analysis

The heat transfer in the hot pin and core average were calculated as specified in the RELAP5 model. The maximum temperatures and lowest heat fluxes were taken from the result and presented for the steady state and reactor shutdown conditions. The use of maximum and minimum values establishes the extreme stresses and heat transfer conditions the VIPR will experience. Using the heat flux in the core compared to the calculated CHF values provides an understanding of the cooling capability of the core. The DNBR is a key parameter used to understand the cooling capability in the core for steady state and accident conditions.

The design of the PCS and the upward flow through the reactor creates the possibility for dynamic flow instability from the creation of voids in the reactor core. The steady state operation between the nominal and limiting configuration is not at risk for flow instabilities. Rapid expansion of the coolant in a heated channel could result in oscillations in the flow through the core. This is a concern when there is significant boiling occurring in the reactor core and a substantial void is generated at low flow rates. The full impact of flow instabilities is seen in the accident scenarios detailed in Chapter 13.

4.6.3.1 Forced Convection Mode

The results from the RELAP5 model of steady state operation are presented in **Table** 4-15. The high DNBR indicates significant boiling can occur before the CHF is reached in the nominal and limiting



AAI-PSAR-04 (NP) Rev 0

Page 4-52

conditions of operation. The cladding and fuel temperatures are within the threshold of the design criteria.

Table 4-15: Thermal-hydraulic characteristics of the VIPR core and hot pin

Parameter		Nominal Configuration				Limiting Configuration			
		Core Average Hot Fuel Pin		Core Average Hot		t Fuel Pin			
Power (MWth)	15			16.8					
Reactor Inlet Coolant Temp. (°C)	[]PROP			[]PROP					
Coolant Saturation Temp. (°C)	[]PROP			[]PROP					
Mass Flow Rate (kg/s)	[] ^{PROP}	[] ^{PROP}	[] ^{PROP}	[] ^{PROP}	
Centerline Fuel Temp. (°C)	[] ^{PROP}	[] ^{PROP}	[] ^{PROP}	[] ^{PROP}	
Cladding Inside Temp. (°C)	[] ^{PROP}	[] ^{PROP}]] ^{PROP}	[] ^{PROP}	
Cladding Surface Temp. (°C)	[] ^{PROP}	[] ^{PROP}	[] ^{PROP}	[] ^{PROP}	
Critical Heat Flux (W/m²)	[] ^{PROP}	[] ^{PROP}	[] ^{PROP}	[] ^{PROP}	
DNBR	[] ^{PROP}]] ^{PROP}]] ^{PROP}	[] ^{PROP}	

There is a significant difference between the hot fuel pin and average fuel pin temperatures, as seen in **Table** 4-15, due to the high radial power peaking factor. During the core operating cycle, the power density and distribution will change with burnup of the fuel and are anticipated to reduce the power peaking factor.

4.6.3.2 Natural Convection Mode

The natural convection mode of operation is intended for shutdown conditions. Passive inlet ports in the plenum remain open between the pool and the reactor core allowing natural circulation to establish. This design allows passive cooling of the core during a shutdown state from either a planned or accident event. The ability to cool the core is subject to the natural circulation path and pool dimensions detailed in Figure 5-5 of Chapter 5. Events that could lead to the shutdown of the reactor are analyzed to ensure safe shutdown and adequate cooling of the core. Anticipated shutdown conditions are analyzed for the limiting core configuration and are presented below.

Planned Shutdown Event

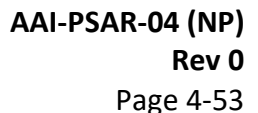
There are anticipated events that would require the planned shutdown of the reactor core. These events follow the following sequence (hh:mm:ss):

00:00:00: Insertion of the control rods

00:15:00: PCS pumps shutoff begins

00:16:42: Pump shutoff complete

00:23:58: Natural circulation is established through the core





Operation of the PCS for 15 minutes removes sufficient decay heat and reduces the fuel, cladding, and coolant to temperatures that can be managed by natural circulation. The transition between forced and natural convection is predicted to be accompanied by a slight increase in the fuel, cladding, and coolant temperatures due to the low decay heat output. This analysis also assumes that flow stopped when the pumps shut down, no coast down is assumed to remain conservative. **Figure 4-29** shows the temperature profile at different locations for the limiting core configuration after shutdown but before forced flow stops. **Figure 4-30** shows how that profile changes when the flow is transitioning from forced flow to natural convection.

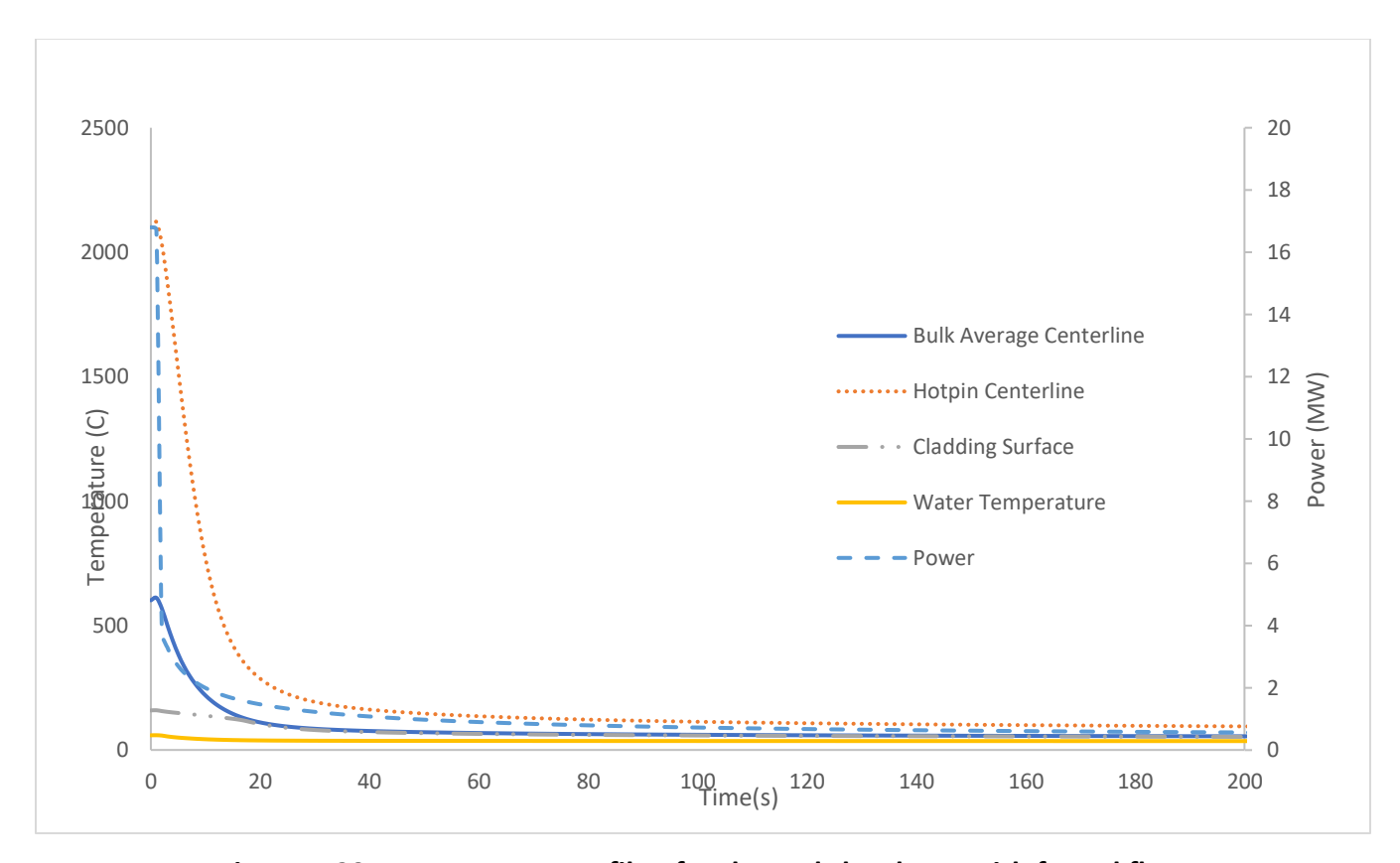


Figure 4-29: Temperature profile of a planned shutdown with forced flow



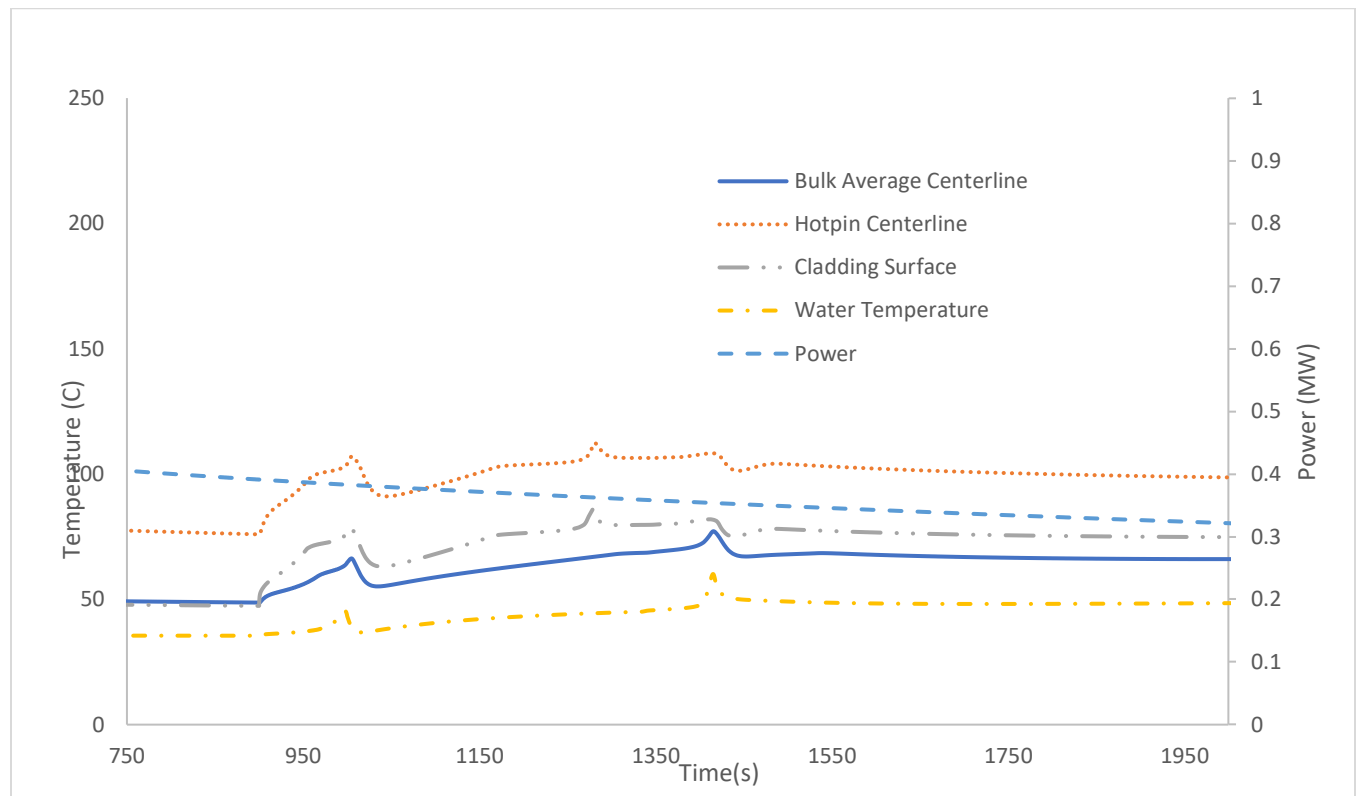


Figure 4-30. Temperature profile transition between forced flow and natural convection

Loss of Power Shutdown Event:

The loss of electrical power is the limiting case for the natural convection mode of cooling the reactor. The ability to maintain sufficient cooling from natural convection alone when the reactor is at full power is considered the bounding case for steady state operation.

The anticipated sequence of events is as follows (mm:ss.ms):

00:00.00: Power is lost to the facility

00:01.00 Insertion of the control rods begins

00:01.00: PCS pumps shut off

00:07.70: Temperature stabilizes and is maintained for 72 hours

The earlier it is in the Loss of Power Shutdown Event the greater the decay heat that must be removed. A higher coolant temperature, compared to the forced convection shutdown case previously discussed, is sustained for a small amount of time until the decay heat from the fuel is reduced and the cooling capacity is maintained by natural convection as shown in **Figure 4-31**.

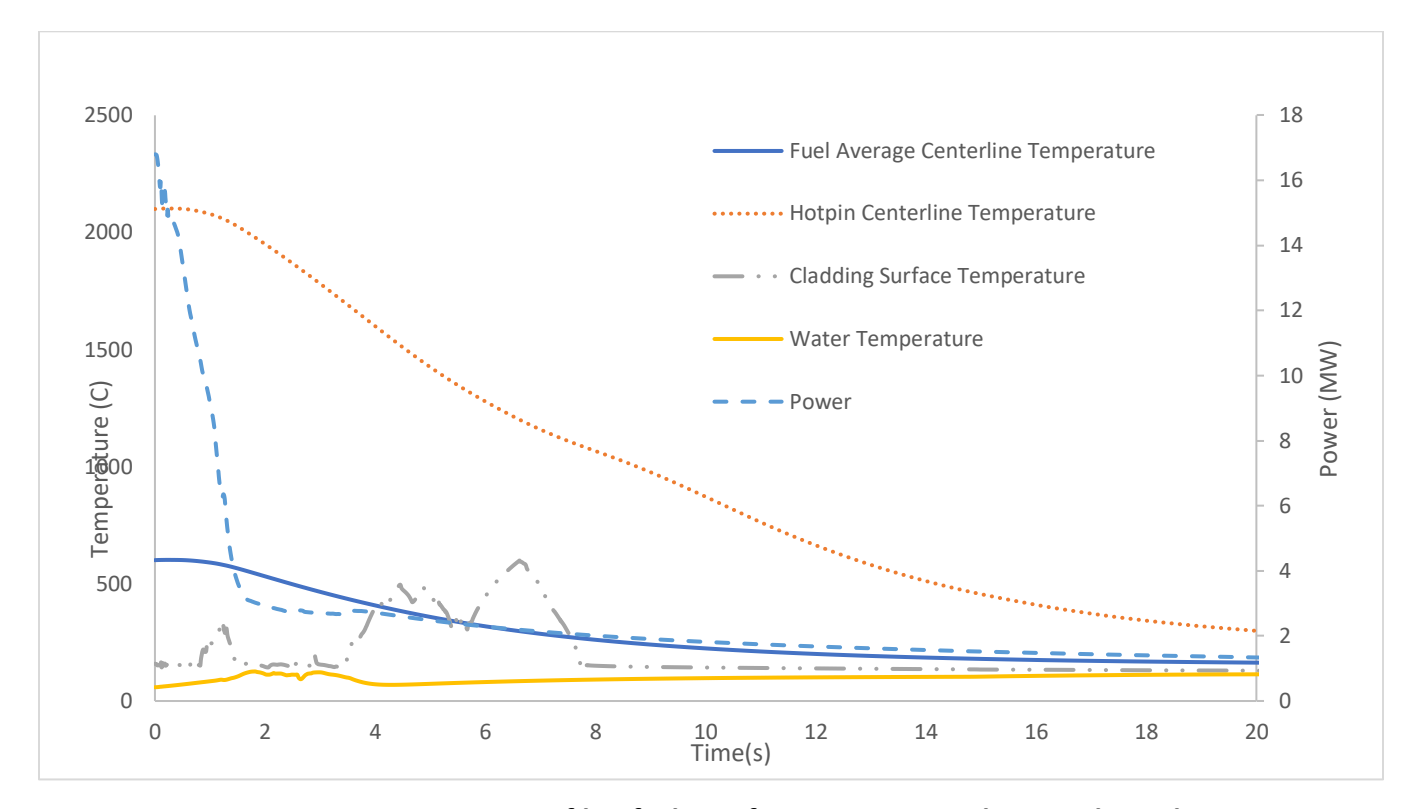


Figure 4-31: Temperature profile of a loss of power event with natural circulation

4.6.3.3 Transients and Power Pulses

The VIPR is not designed for pulsed operation.

The cooling capacity is determined by the limiting core configuration for the following transient conditions:

- Reactor start-up
- Reactor shutdown
- Accident conditions

A full analysis of the thermal-hydraulic performance for each accident is presented in Chapter 13.

4.7 REFERENCES

American Nuclear Society. 2020. ANSI/ANS 6.1.1-2020, "Photon and Neutron Fluence-to-Dose Conversion Coefficients." American National Standards Institute.

Bromley, L. A. 1950. "Heat Transfer in Stable Film Boiling." Chemical Engineering Progress 46: 221-227.

Brown, David A., M. B. Chadwick, R. Capote, A. C. Kahler, A. Trkov, M. W. Herman, A. A. Sonzogni et al., 2018. "ENDF/B-VIII. 0: the 8th major release of the nuclear reaction data library with CIELO-project cross sections, new standards and thermal scattering data." Nuclear Data Sheets 148: 1-142.



AAI-PSAR-04 (NP) Rev 0 Page 4-56

- Chen, J. C. 1966. "A Correlation for Boiling Heat Transfer to Saturated Fluids in Convective Flow." Process Design and Development 5:322-327.
- Chen, J. C., R. K. Sundaram, and F. T. Ozkaynak. 1977. NUREG-0237, "A Phenomenological Correlation for Post-CHF Heat Transfer." (June)
- Churchill, S. W., and H. H. S. Chu. 1975. "Correlating Equations for Laminar and Turbulent Free Convection From a Vertical Plate." *International Journal of Heat and Mass Transfer* 18: 1323-1329.
- Dittus, F. W. and L. M. K. Boelter. 1930. "Heat Transfer in Automobile Radiators of the Tubular Type." *Publications in Engineering* 2: 443-461.
- Groeneveld, D.C., J.Q. Shan, and A.Z. Vasic, et al. 2007. "The 2006 CHF Look-Up Table," *Nuclear Engineering and Design* 237: 1909–1922.
- J. Leppänen, M. Pusa, T. Viitanen, V. Valtavirta, and T. Kaltiaisenaho. "The Serpent Monte Carlo code: Status, development and applications in 2013." Ann. Nucl. Energy, 82 (2015): 142-150.
- Kays, W. M. 1955. "Numerical Solution for Laminar Flow Heat Transfer in Circular Tubes." *Transactions*, American Society of Mechanical Engineers 77 (no.8): 1265-1274.
- McAdams, W. H. 1954. Heat Transmission. 3rd edition. New York: McGraw-Hill.
- National Institute of Standards and Technology. 2025. "Thermophysical Properties of Fluid Systems," NIST Chemistry WebBook, NIST Standard Reference Database Number 69. Gaithersburg MD. https://doi.org/10.18434/T4D303
- Pyecha, T.D., et al. 1985. "Waterside Corrosion of PWR Fuel Rods Through Burnups of 50,000 MWd/MTU", Published in *ANS Topical Meeting on Light Water Reactor Fuel Performance*, Orlando, Florida. (April): 3-17 to 3-55.
- RELAP5 Code Development Team, "RELAP5/MOD3 Code Manual Volume 3: User's Guide and Input Manual."
- RELAP5 Code Development Team, "RELAP5/MOD3 Code Manual Volume 4: Models and Correlations."
- Shah, M. M. 1992. Heat Transfer and Fluid Flow Data Books. Section 507-6: 7. Genium Publishing.
- Sun, K. H., J. M. Gonzales-Santalo, and C. L. Tien. 1976. "Calculations of Combined Radiation and Convection Heat Transfer in Rod Bundles Under Emergency Cooling Conditions." *Journal of Heat Transfer*: 414-420.